Structural Engineering and Mechanics, *Vol. 70, No. 1 (2019) 97-112*
DOI: https://doi.org/10.12989/sem.2019.70.1.097

The effect of porosity on free vibration of SPFG circular plates resting on visco-Pasternak elastic foundation based on CPT, FSDT and TSDT

Ehsan Arshid[1], Ahmad Reza Khorshidvand[*2] and S. Mahdi Khorsandijou[3]

[1]*Department of Solid Mechanics, Faculty of Mechanical Engineering, University of Kashan, Kashan, Iran*
[2]*Department of Mechanical Engineering, South Tehran Branch, Islamic Azad University, Tehran, Iran*
[3]*Department of Mechatronics Engineering, South Tehran Branch, Islamic Azad University, Tehran, Iran*

(Received December 24, 2018, Revised January 27, 2019, Accepted January 29, 2019)

Abstract. Using the classical, first order and third order shear deformation plates theories the motion equations of an undrained porous FG circular plate which is located on visco-Pasternak elastic foundation have been derived and used for free vibration analysis thereof. Strains are related to displacements by Sanders relationship. Fluid has saturated the pores whose distribution varies through the thickness according to three physically probable given functions. The equations are discretized and numerically solved by the generalized differential quadrature method. The effect of porosity, pores distribution, fluid compressibility, viscoelastic foundation and aspect ratio of the plate on its vibration has been considered.

Keywords: free vibration; porous material; circular plate; generalized differential quadrature method; shear deformation plate theory; visco-Pasternak foundation

1. Introduction

The porous material structures are widely used in structural design problems. Technology development in manufacturing materials with functionally graded (FG) properties, especially in aero-spatial and medical industries, has increased the demand for the knowledge describing the behavior of FG structures such as FG beams, plates and shells. It is possible to manufacture FG materials with desired porosities. It is also possible for the pores to have confined gas or fluid with a desired variable pressure. Many natural bodies are in fact functionally graded materials (FGMs) such as stones, wood and layers of soil. The physical and mechanical properties of a porous FGM, namely, electrical conductivity, permeability, tensile strength, are dependent upon the amount of porosity and the distribution type thereof. Biot (1964) was the pioneer who studied poroelasticity, assuming elastically-deformable porous medium as a two-phase continuum composed solid and fluid phases. He introduced some bulk quantities, namely fluid volume change, solid strain components, pressure of the fluid confined in pores and stress components. Biot theory was improved by the concept of partial stresses. Detournay and Cheng (1993) proposed the stress-strain relationship of a porous medium in terms of the elastic constants of solid and fluid phases.

The vibrating and buckling behaviors of porous and FGM structures under the influence of mechanical and thermal loads have been studied and the effects of material properties have been investigated. It is noticeable that each term of the equilibrium equations of an FGM plates is analogous to that of a porous plate. Static and Dynamic Stability of FG Plates and Shells considered by Duc (2014). Nonlinear bending and post-buckling of circular FG plates subjected to mechanical and thermal loads has been studied by Ma and Wang (2003a, 2003b, 2004) on the basis of the first and third order shear deformation theories. Cong *et al.* (2018) considered nonlinear thermo-mechanical buckling and post-buckling response of porous FGM plates using Reddy's high order shear deformation plate theory (HSDT). Nonlinear dynamic response of FGM porous plates on elastic foundation subjected to thermal and mechanical loads using the first order shear deformation theory (FSDT) studied by Duc *et al.* (2018). In another study Duc *et al.* (2018) considered thermal buckling of FGM sandwich truncated conical shells reinforced by FGM stiffeners on elastic foundations. They used the FSDT to analyze the structure. Nonlinear dynamic analysis and vibration of eccentrically stiffened FGM elliptical cylindrical shells carried out by Duc *et al.* (2017). Free and forced nonlinear vibrations of an axisymmetric thin circular FG plate have been analyzed by Allahverdizadeh *et al.* (2008) via semi-analytical approaches entitled Kantorovich time averaging technique and assumed-time-mode method. The free vibration or the so-called natural frequencies appear dependent on initial conditions. Moreover, the response characteristics are significantly influenced by the volume fraction of the plate. Duc (2016) employed Reddy's third order shear deformation theory (TSDT) to analyze nonlinear thermal dynamic behavior of eccentrically stiffened sigmoid power law distribution FGM circular cylindrical shells surrounded on elastic foundations. Nonlinear dynamic response of a doubly curved imperfect

∗Corresponding author, Assistant Professor
E-mail: Ar_Khorshidvand@azad.ac.ir

ISSN: 1225-4568 (Print), 1598-6217 (Online)

FGM shell investigated by Duc (2013). He studied effect of different parameters such as imperfection, materials distribution and elastic foundation on the results. Thermo-electro-mechanical dynamic response of shear deformable piezoelectric sigmoid FG sandwich circular cylindrical shells presented by Duc (2018). He took the nonlinear terms into account based on Von-Karman relations and considered effect of temperature on the material properties. Thin FGM doubly curved shells dynamic behavior studied by Duc and Quan (2015). They assumed that the shell is located on elastic foundation. Quan *et al.* (2015) investigated cylindrical panels with metal-ceramic-metal layers vibration and dynamic analyses. Based on the classical plate theory (CPT), a thermoelastic buckling analysis of FG circular plates integrated with piezoelectric layers has been presented by Khorshidvand *et al.* (2012). Using the FSDT, the solutions for deflections and force and moment resultants in axisymmetric bending and stretching of FG circular and annular plates have been achieved by Reddy *et al.* (1999). On the basis of FSDT, free vibration of circular plates has been studied by Wu *et al.* (2002) from the vantage of the generalized differential quadrature (GDQ) method. The relationship between amplitude and frequency ratio in the forced nonlinear vibration of circular plates subjected to different loads and supports has been obtained by Decha-Umphai and Mei (1986) through finite element method. In vibration and buckling analysis of laminated isotropic annular plates, closed-form solutions for the mode shapes have been achieved by Krizhevsky and Stavsky (1996) in terms of the transcendental functions, namely Bessel, trigonometric and power ones. The effects of transverse shear deformation, rotary inertia and boundary conditions on the results have been found. Buckling, bending and free vibration analyses of thin isotropic plates and columns have been given by Civalek (2004) applying DQ and harmonic differential quadrature (HDQ) methods. For a few number of the plate shapes and boundary conditions, it was shown that the results of HDQ will be more accurate than those of DQ method, if the number of the grid points is held the same. Nonlinear bending of thin rectangular orthotropic plates undergoing large elastic deflections with immovable edges has been analyzed by Bert *et al.* (1989) via the differential quadrature method (DQM). The results have been compared with analytical and experimental ones. Nonlinear vibration of a shear deformable FG plate was presented by Chen (2005) when the material properties were considered to change continuously through thickness. The governing nonlinear partial differential equations (PDEs) were transformed into ordinary differential equations by means of the Galerkin method. The linear and nonlinear natural frequencies were obtained by applying the Runge-Kutta methods. In accordance with the three-dimensional elasticity theory, the free vibration of FGM axisymmetric circular plates has been studied by Wang *et al.* (2009). The material properties were considered to vary across thickness according to a given exponential function. Imperfect shells and circular plates with free edges have been taken into consideration by Camier *et al.* (2009) for nonlinear vibration analyses. The motion equations were derived by using the dynamic analog

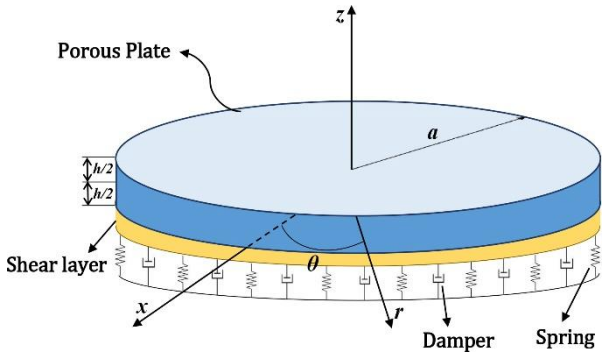

Fig. 1 The scheme of circular FG plate made of saturated porous materials resting on visco-Pasternak elastic foundation

of the von-Karman equations for an initially-perfect thin plate. This way sounds to be accurate enough to analyze shallow shells assumed as an imperfect plate. The natural frequencies of a ferro-magnetic beam with a circular cross section have been computed by Wang (2008) utilizing Zhou-Zheng's energy method. He has also presented a dynamical model for predicting the behavior of the beam subjected to a transverse magnetic field. Stability analysis of imperfect three-phase sandwich laminated panels in thermal environments presented by Thu and Duc (2016). They used Von-Karman nonlinear terms for their analysis and used analytical approach to obtain the results. Also bending analysis of thin composite simply supported edges plate under steady temperature field considered by Duc and Ha (2011). They used the Navier's solution method to obtain the results. Effect of multi physical fields on vibration of double-bonded sandwich microplates studied by Mohammadimehr *et al.* (2017). Ghorbanpour Arani *et al.* (2017a, 2017b) in two researches investigated vibrational behavior of FG nanocomposite plates which was moving in two directions.

By reviewing the literature, it is found that there is not any researches about vibration of a saturated porous functionally graded (SPFG) plate located on visco-elastic foundation based on various shear deformation plates theories. So, in the present paper, the motion equations of a circular porous FG plate have been obtained using the Hamilton's principle. Although the effects of shear deformability of the plate have been neglected according to the CPT, but it is taken into account using FSD and TSD theories. The mechanical properties of the porous plate are assumed to change through thickness. The plate motion equations were numerically solved through GDQ method for clamped and simply supported boundary conditions, to find the effect of radius, thickness, pore compressibility, porosity parameter and distributions and also visco-Pasternak foundation constants on the natural frequencies and mode shapes of the plate. The results of the current research will help to improve the structures mechanical behaviors and design them such a way to achieve the desired results.

2. Plate properties

Fig. 1 shows a perfect uniform circular plate made of a saturated porous material with radius a and thickness h which is rested on visco-Pasternak elastic foundation. The origin and two axes of the illustrated cylindrical coordinate reference frame (r,θ,z) are located in the middle plane of the plate.

The porous material properties are assumed to vary through thickness. The shear modulus of elasticity and the density of the plate have been considered functions of porosity parameter e_1 and mass density coefficient e_m, and vary through the thickness of the plate in accordance with functions represented by either Eq. (1) for non-symmetric, Eq. (2) for symmetric or Eq. (3) for monotonous porosity distribution (Magnucka-Blandzi 2008)

$$\frac{G(z)}{G_0} = 1 - e_1 \cos\left(\frac{\pi z}{2h} + \frac{\pi}{4}\right), \qquad \frac{\rho(z)}{\rho_0} = 1 - e_m \cos\left(\frac{\pi z}{2h} + \frac{\pi}{4}\right) \tag{1}$$

At the upper and lower layers of the plate, the shear moduli of elasticity are denoted by G_0 and G_1, and the densities are denoted by ρ_0 and ρ_1, respectively. According to Ref. (Khorshidvand *et al*. 2014), G_1 is equal or less than G_0.

$$\frac{G(z)}{G_0} = 1 - e_1 \cos\left(\frac{\pi z}{h}\right), \qquad \frac{\rho(z)}{\rho_0} = 1 - e_m \cos\left(\frac{\pi z}{h}\right) \tag{2}$$

For the symmetric porosity distribution, the shear moduli of elasticity at the upper and lower layers, as well as the densities, are the same (G_1=G_0 and ρ_1=ρ_0).

$$\frac{G(z)}{G_0} = 1 - e_1 \chi, \qquad \frac{\rho(z)}{\rho_0} = \sqrt{1 - e_1 \chi} \tag{3}$$

where

$$\chi = \frac{1}{e_1} - \frac{1}{e_1}\left(\frac{2}{\pi}\sqrt{1-e_1} - \frac{2}{\pi} + 1\right)^2 \tag{4}$$

The plate's porosity parameter, i.e., e_1, represents the void to bulk volume ratio. It is defined by Eq. (5) and is greater than zero and smaller than one.

$$e_1 = 1 - \frac{G_1}{G_0} = 1 - \frac{E_1}{E_0} \tag{5}$$

The mass density coefficient is presented by e_m which is related to porosity coefficient using the following relation (Amir *et al*. 2018a)

$$e_m = 1 - \sqrt{1 - e_1} \tag{6}$$

The mentioned coefficient can also be defined using the densities of the upper and lower layers as

$$e_m = 1 - \frac{\rho_1}{\rho_0} \tag{7}$$

It is well-know that the modulus of elasticity E is equal to $2G(1+\nu)$ where G is the shear modulus and ν is the Poisson's ratio. Despite G and E, the Poisson's ratio is assumed constant with respect to z.

Based on the linear poroelasticity theory of Biot (Biot 1964), increase of pressure of the fluid confined by the pores, causes dilatation or positive volumetric strain in the pores, and compression of the pores increases the pressure of the fluid. As a result, the stress-strain relationship for poroelastic FG materials is given by Eq. (8) within which σ_{ij} and ε_{ij} are the stress and strain components, respectively (Detournay and Cheng 1993). δ_{ij} is the Kronecker delta, ε is the volumetric strain, P is the pressure of fluid confined by the pores and ν_u is the undrained Poisson's ratio. It should be noted that ν_u is greater than ν and less than 0.5.

$$\sigma_{ij} = 2G(z)\varepsilon_{ij} + \frac{2G(z)\nu_u}{1-2\nu_u}\varepsilon\delta_{ij} - \alpha P\delta_{ij} \tag{8}$$

Pressure of the fluid confined by the pores is given by Eq. (9) where M is the Biot's modulus, ξ is the fluid volume change and α is the Biot's coefficient of effective or volumetric strain.

$$P = M(\xi - \alpha\varepsilon) \tag{9}$$

It should be noted that α is greater than zero and less than one. In undrained state, the effects of porosity and generated pore stress on the solid phase of a poroelastic material are indicated by Biot coefficient.

Biot's modulus is given by Eq. (10)

$$M = \frac{2G(z)(\nu_u - \nu)}{\alpha^2(1-2\nu_u)(1-2\nu)} \tag{10}$$

Undrained Poisson's ratio is given by Eq. (11) where B is the Skempton number

$$\nu_u = \frac{\nu + \alpha B(1-2\nu)/3}{1 - \alpha B(1-2\nu)/3} \tag{11}$$

In undrained status, the effect of pressure of the pore fluid on the behavior of a poroelastic material, is taken into consideration by this dimensionless number. Skempton number is defined by Eq. (14) as the rate of change of fluid pressure with respect to the trace of the stress tensor.

As a matter of fact, Poisson's ratio is defined as the magnitude of strain ratio of lateral to axial strains. Because the deformations of a poroelastic material are different in drained and undrained conditions, the drained and undrained Poisson's ratios have been defined by Eqs. (12) and (13), respectively

$$\nu = -\frac{\varepsilon_{lateral}}{\varepsilon_{axial}}, \qquad [\sigma] = \begin{bmatrix} \sigma_{Axial} & 0 & 0 \\ 0 & 0 & 0 \\ 0 & 0 & 0 \end{bmatrix}, \qquad P = 0 \tag{12}$$

$$\nu_u = -\frac{\varepsilon_{lateral}}{\varepsilon_{axial}}, \qquad [\sigma] = \begin{bmatrix} \sigma_{Axial} & 0 & 0 \\ 0 & 0 & 0 \\ 0 & 0 & 0 \end{bmatrix}, \qquad \xi = 0 \tag{13}$$

Skempton number is an important dimensionless parameter to describe the effect of the fluid in the pores on the behavior of porous material in undrained state (ξ=0) and is described as the ratio of the pores pressure to total body volumetric stress

$$B=\frac{dp}{d\sigma}=\frac{1}{1+e_1^{C_p/C_s}}=\frac{K_u-K}{\alpha K_u},\qquad \xi=0 \tag{14}$$

In Eq. (14) the drained and undrained bulk moduli, are represented by K and K_u, respectively. Bulk modulus indicates the compressibility of a material. Bulk moduli of a poroelastic material in drained and undrained conditions are given by the well-known Eqs. (15)-(16), respectively. C_p and C_s represent the compressibility of fluid and solid phases of a poroelastic material. According to Eq. (14) Skempton number indicates how fluid compressibility influences on the elastic modulus and compressibility of a poroelastic material.

$$K=\frac{2(1+\nu)}{3(1-2\nu)}G, \tag{15}$$

$$K_u=\frac{2(1+\nu_u)}{3(1-2\nu_u)}G \tag{16}$$

The two dimensional stress-strain law, for plane stress undrained status, is given by Eq. (17) in cylindrical coordinate reference frame (Jabbari *et al*. 2014)

$$\begin{aligned}
\sigma_{rr}&=A_1(z)\varepsilon_{rr}+B_1(z)\varepsilon_{\theta\theta},\\
\sigma_{\theta\theta}&=A_1(z)\varepsilon_{\theta\theta}+B_1(z)\varepsilon_{rr},\\
\sigma_{r\theta}&=G(z)\gamma_{r\theta},\\
\sigma_{rz}&=G(z)\gamma_{rz},\\
\sigma_{\theta z}&=G(z)\gamma_{\theta z}
\end{aligned} \tag{17}$$

where (Arshid and Khorshidvand 2018)

$$\begin{aligned}
A_1&=\left(\frac{2}{1-\nu_u^2}\right)\left[1+\nu_u+\frac{(\nu_u-\nu)(1+\nu_u)}{1-2\nu}\left(1-\frac{C_2}{C_1}\right)\right]G(z),\\
B_1&=\left(\frac{2}{1-\nu_u^2}\right)\left[(1+\nu_u)\nu_u+\frac{(\nu_u-\nu)(1+\nu_u)}{1-2\nu}\left(1-\frac{C_2}{C_1}\right)\right]G(z)
\end{aligned} \tag{18}$$

in which

$$\begin{aligned}
C_1&=2\left[1+\frac{\nu_u}{1-2\nu_u}+\frac{\nu_u-\nu}{(1-2\nu_u)(1-2\nu)}\right]G(z),\\
C_2&=C_1-2G(z)
\end{aligned} \tag{19}$$

3. Kinematic relations

In this study, three different plate's theories namely CPT, FSDT and TSDT are investigated to describe the displacement components.

3.1 CPT

According to the CPT and the Love-Kirchhoff hypothesis (Reddy 2004), the displacement components are described using the following expressions (Arefi and Zenkour 2017)

$$\begin{aligned}
u(r,\theta,z,t)&=u_0(r,\theta,t)-z\frac{\partial w_0(r,\theta,t)}{\partial r},\\
v(r,\theta,z,t)&=v_0(r,\theta,t)-\frac{z}{r}\frac{\partial w_0(r,\theta,t)}{\partial \theta},\\
w(r,\theta,z,t)&=w_0(r,\theta,t)
\end{aligned} \tag{20}$$

where u, v and w are displacement of each point of the plate in r, θ and z directions and u_0, v_0 and w_0 are those of related to middle plane of the plate.

3.2 FSDT

The displacements are described according to FSDT as below (Amir *et al*. 2018b, Ozdemir 2018)

$$\begin{aligned}
u(r,\theta,z,t)&=u_0(r,\theta,t)+z\varphi_r(r,\theta,t),\\
v(r,\theta,z,t)&=v_0(r,\theta,t)+z\varphi_\theta(r,\theta,t),\\
w(r,\theta,z,t)&=w_0(r,\theta,t)
\end{aligned} \tag{21}$$

in which φ_r and φ_θ are the rotations of the mid-surface about θ and r axes, respectively.

3.3 TSDT

TSDT is one of the most popular HSDTs which also called as Reddy's theory. Generally, higher order theories present the kinematics better and lead to more accurate results without using any shear correction factor (Ghorbanpour Arani *et al*. 2016, El-Haina *et al*. 2017). But the equations and computational are more difficult than the lower order theories. Since the difference between the results of TSD and higher than third order theories are negligible and due to avoiding complicated equations and more CPU time usage, TSDT is employed to obtain the results with high accuracy. Based on TSDT the displacement components of the considering plate are described as (Ghorbanpour Arani *et al*. 2017c)

$$\begin{aligned}
u(r,\theta,z,t)&=u_0(r,\theta,t)+z\varphi_r(r,\theta,t)-c_1z^3\left[\varphi_r(r,\theta,t)+\frac{\partial w_0(r,\theta,t)}{\partial r}\right],\\
v(r,\theta,z,t)&=v_0(r,\theta,t)+z\varphi_\theta(r,\theta,t)-c_1z^3\left[\varphi_\theta(r,\theta,t)+\frac{1}{r}\frac{\partial w_0(r,\theta,t)}{\partial \theta}\right],\\
w(r,\theta,z,t)&=w_0(r,\theta,t)
\end{aligned} \tag{22}$$

where

$$c_1 = \frac{4}{3h^2} \tag{23}$$

3.4 Strain-displacement relations

The general relations between the non-zero strain and displacement components in cylindrical coordinate system on the basis of Sanders assumptions (Brush et al., 1975) and regarding the Von-Karman relations, are presented as follows

$$\varepsilon_{rr} = \frac{\partial u}{\partial r} + \frac{1}{2}\left(\frac{\partial w}{\partial r}\right)^2,$$

$$\varepsilon_{\theta\theta} = \frac{1}{r}\frac{\partial v}{\partial \theta} + \frac{u}{r} + \frac{1}{2}\left(\frac{1}{r}\frac{\partial w}{\partial \theta}\right)^2,$$

$$\gamma_{r\theta} = \frac{1}{r}\frac{\partial u}{\partial \theta} - \frac{v}{r} + \frac{\partial v}{\partial r} + \frac{1}{r}\left(\frac{\partial w}{\partial \theta}\right)\left(\frac{\partial w}{\partial r}\right), \tag{24}$$

$$\gamma_{rz} = \frac{\partial u}{\partial z} + \frac{\partial w}{\partial r} + \left(\frac{\partial w}{\partial z}\right)\left(\frac{\partial w}{\partial r}\right),$$

$$\gamma_{\theta z} = \frac{\partial v}{\partial z} + \frac{1}{r}\frac{\partial w}{\partial \theta} + \frac{1}{r}\left(\frac{\partial w}{\partial \theta}\right)\left(\frac{\partial w}{\partial z}\right)$$

Noted that by substituting the CPT, FSDT and TSDT displacement fields into the strains of Eq. (24), the strain-displacement relations for each theory can be obtained.

4. Motion equations and boundary conditions

The governing motion equations and boundary conditions are derived by applying the Hamilton's principle given by Eq. (25) within which *U* and *T* are respectively the elastic strain and kinetic energies of the plate and *W* is the work of the non-conservative loads which is due to viscoelastic foundation in the present study (Bennoun *et al*. 2016, Zenkour 2018)

$$\int_{t_1}^{t_2}\left[(\delta U - \delta W) - \delta T\right] \mathrm{d}t = 0 \tag{25}$$

The elastic strain energy of a saturated porous FG circular plate is given by Eq. (26) as follows (Arshid and Khorshidvand 2017, Yahiaoui *et al*. 2018, Kolahdouzan *et al*. 2018)

$$U = \frac{1}{2}\int_{-h/2}^{h/2}\int_0^{2\pi}\int_0^{r}(\sigma_{rr}\varepsilon_{rr} + \sigma_{\theta\theta}\varepsilon_{\theta\theta} + \sigma_{r\theta}\gamma_{r\theta} + \sigma_{rz}\gamma_{rz} + \sigma_{\theta z}\gamma_{\theta z})\, r\,\mathrm{d}r\,\mathrm{d}\theta\,\mathrm{d}z \tag{26}$$

And the kinetic energy thereof is given by Eq. (27) (Loghman and Cheraghbak 2018)

$$T = \frac{1}{2}\int_{-h/2}^{h/2}\int_0^{2\pi}\int_0^{r}\rho(z)\left[\left(\frac{\partial u}{\partial t}\right)^2 + \left(\frac{\partial v}{\partial t}\right)^2 + \left(\frac{\partial w}{\partial t}\right)^2\right] r\,\mathrm{d}r\,\mathrm{d}\theta\,\mathrm{d}z \tag{27}$$

The external work due to visco-Pasternak foundation can be expressed as (Duc *et al*. 2017, Belmahi *et al*. 2018)

$$W = \frac{1}{2}\int_0^{2\pi}\int_0^{r}\left[F.w(r,\theta,t)\right] r\,\mathrm{d}r\,\mathrm{d}\theta \tag{28}$$

where *F* is the force of viscoelastic foundation and is as follow (Amir 2016, Ghorbanpour Arani and Kiani 2018)

$$F = K_W w(r,\theta,t) + C_d\frac{\partial w(r,\theta,t)}{\partial t} - K_G\nabla^2 w(r,\theta,t) \tag{29}$$

Here, K_W, K_G and C_d are the Winkler, shear layer and damping constants, respectively.

$$\nabla^2 w(r,\theta,t) = \frac{\partial^2 w(r,\theta,t)}{\partial r^2} + \frac{1}{r}\frac{\partial w(r,\theta,t)}{\partial r} + \frac{1}{r^2}\frac{\partial^2 w(r,\theta,t)}{\partial \theta^2} \tag{30}$$

Substituting Eqs. (26)-(28) into Eq. (25), performing by-part integrations and mathematical simplification, the linearized motion Equations and boundary conditions in axisymmetric condition which makes them simpler are achieved based on CP, FSD and TSD theories as follows:

4.1 Equations based on CPT

The governing equations according to CPT are obtained as follows

δu_0 :

$$\begin{aligned} &rA_{10}\frac{\partial^2 u_0}{\partial r^2} + A_{10}\frac{\partial u_0}{\partial r} - \frac{A_{10}}{r}u_0 - rA_{11}\frac{\partial^3 w_0}{\partial r^3} - A_{11}\frac{\partial^2 w_0}{\partial r^2} \\ &\quad + \frac{A_{11}}{r}\frac{\partial w_0}{\partial r} - rI_0\frac{\partial^2 u_0}{\partial t^2} = 0 \end{aligned} \tag{31}$$

δw_0 :

$$\begin{aligned} &rA_{11}\frac{\partial^3 u_0}{\partial r^3} + 2A_{11}\frac{\partial^2 u_0}{\partial r^2} - \frac{A_{11}}{r}\frac{\partial u_0}{\partial r} + \frac{A_{11}}{r^2}u_0 - rA_{12}\frac{\partial^4 w_0}{\partial r^4} \\ &\quad -2A_{12}\frac{\partial^3 w_0}{\partial r^3} + \frac{A_{12}}{r}\frac{\partial^2 w_0}{\partial r^2} - rK_G\frac{\partial^2 w_0}{\partial r^2} - \frac{A_{12}}{r^2}\frac{\partial w_0}{\partial r} \\ &\quad -K_G\frac{\partial w_0}{\partial r} + rK_w w_0 + rC_d\frac{\partial w_0}{\partial t} - rI_0\frac{\partial^2 w_0}{\partial t^2} = 0 \end{aligned} \tag{32}$$

Also, the boundary conditions corresponding to clamped support of a circular plate at outer edge, i.e. at $r=a$, are given by Eqs. (33)

$$u_0 = 0, \qquad w_0 = 0, \qquad \frac{\partial w_0}{\partial r} = 0 \tag{33}$$

At outer edge, i.e. at $r=a$, the boundary conditions corresponding to simple support thereof are given by Eqs. (34)

$$u_0 = 0, \qquad w_0 = 0, \qquad M_{rr} = 0 \tag{34}$$

Independent of Hamilton's principle, the continuity conditions at the center of the circular plate is given by Eqs. (35)

$$u_0 = 0, \qquad \frac{\partial w_0}{\partial r} = 0, \qquad \frac{1}{r}\frac{\partial^2 w_0}{\partial r^2} + \frac{\partial^3 w_0}{\partial r^3} = 0 \tag{35}$$

Due to the fact that the equations are singular at the plate center, i.e., at $r=0$, a non-zero small value is assigned for *r* in numerical computations of the current research.

4.2 Equations based on FSDT

Employing FSDT displacement field, leads to achieve the following governing equations

$$\delta u_0:$$

$$A_{10}r\frac{\partial^2 u_0}{\partial r^2}+A_{10}\frac{\partial u_0}{\partial r}-\frac{1}{r}A_{10}u_0+A_{11}r\frac{\partial^2\varphi_r}{\partial r^2}+A_{11}\frac{\partial\varphi_r}{\partial r}-\frac{1}{r}A_{11}\varphi_r-rI_0\frac{\partial^2 u_0}{\partial t^2}-rI_1\frac{\partial^2\varphi_r}{\partial t^2}=0 \tag{36}$$

$$\delta w_0:$$

$$r\kappa_f G_{10}\frac{\partial^2 w_0}{\partial r^2}-rK_G\frac{\partial^2 w_0}{\partial r^2}+\kappa_f G_{10}\frac{\partial w_0}{\partial r}-K_G\frac{\partial w_0}{\partial r}+rK_W w_0+r\kappa_f G_{10}\frac{\partial\varphi_r}{\partial r}+\kappa_f G_{10}\varphi_r+rC_d\frac{\partial w_0}{\partial t}-rI_0\frac{\partial^2 w_0}{\partial t^2}=0 \tag{37}$$

$$\delta\varphi_r:$$

$$A_{11}r\frac{\partial^2 u_0}{\partial r^2}+A_{11}\frac{\partial u_0}{\partial r}-\frac{1}{r}A_{11}u_0-\kappa_f rG_{10}\frac{\partial w_0}{\partial r}+A_{12}r\frac{\partial^2\varphi_r}{\partial r^2}+A_{12}\frac{\partial\varphi_r}{\partial r}-\frac{1}{r}A_{12}\varphi_r-\kappa_f rG_{10}\varphi_r-rI_1\frac{\partial^2 u_0}{\partial t^2}-rI_2\frac{\partial^2\varphi_r}{\partial t^2}=0 \tag{38}$$

where κ_f is the shear correction factor and for the circular plate is equal to $\pi^2/12$.

And for a clamped edge circular plate, the boundary condition is

$$u_0=0,\qquad w_0=0,\qquad \varphi_r=0 \tag{39}$$

Also, for simple supports edge, they can be written as

$$u_0=0,\qquad w_0=0,\qquad M_{rr}=0 \tag{40}$$

And the continuity conditions at the center of the plate are as

$$u_0=0,\qquad \frac{\partial w_0}{\partial r}=0,\qquad \varphi_r=0 \tag{41}$$

4.3 Equations based on TSDT

Using the TSDT, the following governing equations are obtained as

$$\delta u_0:$$

$$rA_{10}\frac{\partial^2 u_0}{\partial r^2}+A_{10}\frac{\partial u_0}{\partial r}-\frac{A_{10}}{r}u_0-rA_{13}c_1\frac{\partial^3 w_0}{\partial r^3}-A_{13}c_1\frac{\partial^2 w_0}{\partial r^2}+\frac{A_{13}c_1}{r}\frac{\partial w_0}{\partial r}-\left(-rA_{11}+rA_{13}c_1\right)\frac{\partial^2\varphi_r}{\partial r^2}-A_{13}c_1\frac{\partial\varphi_r}{\partial r}+A_{11}\frac{\partial\varphi_r}{\partial r}-\left(\frac{A_{11}}{r}-\frac{A_{13}c_1}{r}\right)\varphi_r-rI_0\frac{\partial^2 u_0}{\partial t^2}+c_1I_3r\frac{\partial^3 w_0}{\partial t^2\partial r}+c_1I_4r\frac{\partial^2\varphi_r}{\partial t^2}-rI_1\frac{\partial^2\varphi_r}{\partial t^2}=0 \tag{42}$$

$$\delta w_0: \tag{43}$$

$$c_1rA_{13}\frac{\partial^3 u_0}{\partial r^3}+2c_1A_{13}\frac{\partial^2 u_0}{\partial r^2}-\frac{c_1A_{13}}{r}\frac{\partial u_0}{\partial r}+\frac{c_1A_{13}}{r^2}u_0-c_1^2rA_{16}\frac{\partial^4 w_0}{\partial r^4}-2c_1^2A_{16}\frac{\partial^3 w_0}{\partial r^3}+\left(\frac{c_1^2A_{16}}{r}+9c_1^2rG_{14}-6rG_{12}c_1+rG_{10}+rK_G\right)\frac{\partial^2 w_0}{\partial r^2}-\left(-G_{10}+\frac{c_1^2A_{16}}{r^2}+6c_1G_{12}-9c_1^2G_{14}-K_G\right)\frac{\partial w_0}{\partial r}+rK_W w_0+\left(c_1rA_{14}-c_1^2rA_{16}\right)\frac{\partial^3\varphi_r}{\partial r^3}-\left(2c_1^2A_{16}-2c_1A_{14}\right)\frac{\partial^2\varphi_r}{\partial r^2}-\left(-9c_1^2rG_{14}-\frac{c_1^2A_{16}}{r}+\frac{c_1A_{14}}{r}+6rG_{12}c_1-rG_{10}\right)\frac{\partial\varphi_r}{\partial r}-\left(\frac{c_1^2A_{16}}{r^2}-G_{10}-\frac{c_1A_{14}}{r^2}-9c_1^2G_{14}+6c_1G_{12}\right)\varphi_r+rC_d\frac{\partial w_0}{\partial t}-c_1I_3r\frac{\partial^3 u_0}{\partial t^2\partial r}-c_1I_3\frac{\partial^2 u_0}{\partial t^2}+c_1^2I_6r\frac{\partial^4 w_0}{\partial t^2\partial r^2}+c_1^2I_6\frac{\partial^3 w_0}{\partial t^2\partial r}-rI_0\frac{\partial^2 w_0}{\partial t^2}+c_1^2I_6r\frac{\partial^3\varphi_r}{\partial t^2\partial r}-c_1I_4r\frac{\partial^2\varphi_r}{\partial t^2\partial r}-c_1I_4\frac{\partial^2\varphi_r}{\partial t^2}+c_1^2I_6\frac{\partial^2\varphi_r}{\partial t^2}=0$$

$$\delta\varphi_r:$$

$$\left(rA_{11}-c_1rA_{13}\right)\frac{\partial^2 u_0}{\partial r^2}-\left(c_1A_{13}-A_{11}\right)\frac{\partial u_0}{\partial r}-\left(\frac{A_{11}}{r}-\frac{c_1A_{13}}{r}\right)u_0+\left(c_1^2rA_{16}-rA_{14}c_1\right)\frac{\partial^3 w_0}{\partial r^3}-\left(A_{14}c_1-c_1^2A_{16}\right)\frac{\partial^2 w_0}{\partial r^2}-\left(9c_1^2rG_{14}+\frac{c_1^2A_{16}}{r}-6c_1rG_{12}-\frac{A_{14}c_1}{r}+rG_{10}\right)\frac{\partial w_0}{\partial r}+\left(rA_{12}+c_1^2rA_{16}-2c_1rA_{14}\right)\frac{\partial^2\varphi_r}{\partial r^2}-\left(2A_{14}c_1-c_1^2A_{16}-A_{12}\right)\frac{\partial\varphi_r}{\partial r}-\left(-6c_1rG_{12}+rG_{10}-\frac{2c_1A_{14}}{r}+9c_1^2rG_{14}+\frac{c_1^2A_{16}}{r}+\frac{A_{12}}{r}\right)\varphi_r-rI_1\frac{\partial^2 u_0}{\partial t^2}+c_1I_3r\frac{\partial^2 u_0}{\partial t^2}-c_1^2I_6r\frac{\partial^3 w_0}{\partial t^2\partial r}+c_1I_4r\frac{\partial^3 w_0}{\partial t^2\partial r}-rI_2\frac{\partial^2\varphi_r}{\partial t^2}-c_1^2I_6r\frac{\partial^2\varphi_r}{\partial t^2}+2c_1I_4r\frac{\partial^2\varphi_r}{\partial t^2}=0 \tag{44}$$

Unlike the CPT and FSDT, TSDT needs four conditions for each clamped or simple supports edge circular plate. The boundary conditions of a clamped edge circular plate are as

$$u_0=0,\qquad w_0=0,\qquad \frac{\partial w_0}{\partial r}=0,\qquad \varphi_r=0 \tag{45}$$

And simple supports edge plate conditions can be written

$$u_0=0,\qquad w_0=0,$$

$$-c_1rA_{13}\frac{\partial u_0}{\partial r}-c_1rA_{14}\frac{\partial\varphi_r}{\partial r}+c_1^2rA_{16}\frac{\partial\varphi_r}{\partial r}+c_1^2rA_{16}\frac{\partial^2 w_0}{\partial r^2}-c_1B_{13}u_0-c_1B_{14}\varphi_r+c_1^2B_{16}\varphi_r+c_1^2B_{16}\frac{\partial w_0}{\partial r}=0,$$

$$rA_{11}\frac{\partial u_0}{\partial r}+rA_{12}\frac{\partial\varphi_r}{\partial r}-c_1rA_{14}\frac{\partial\varphi_r}{\partial r}-c_1rA_{14}\frac{\partial^2 w_0}{\partial r^2}+B_{11}u_0+B_{12}\varphi_r-c_1B_{14}\varphi_r-c_1B_{14}\frac{\partial w_0}{\partial r}-c_1rA_{13}\frac{\partial u_0}{\partial r}-c_1rA_{14}\frac{\partial\varphi_r}{\partial r}+c_1^2rA_{16}\frac{\partial\varphi_r}{\partial r}+c_1^2rA_{16}\frac{\partial^2 w_0}{\partial r^2}-c_1B_{13}u_0-c_1B_{14}\varphi_r+c_1^2B_{16}\varphi_r+c_1^2B_{16}\frac{\partial w_0}{\partial r}=0 \tag{46}$$

The center of the plate continuity condition are expressed as

$$u_0 = 0, \qquad \frac{\partial w_0}{\partial r} = 0, \qquad \varphi_r = 0,$$

$$\begin{aligned}
&-3c_1 rG_{12}\varphi_r + 3c_1^2 rG_{14}\varphi_r + 3c_1^2 rG_{14}\frac{\partial w_0}{\partial r} - 3c_1 rG_{12}\frac{\partial w_0}{\partial r} + c_1 A_{13}\frac{\partial u_0}{\partial r}\\
&+c_1 A_{14}\frac{\partial \varphi_r}{\partial r} - c_1^2 A_{16}\frac{\partial \varphi_r}{\partial r} - c_1^2 A_{16}\frac{\partial^2 w_0}{\partial r^2} + c_1 rA_{13}\frac{\partial^2 u_0}{\partial r^2} + c_1 rA_{14}\frac{\partial^2 \varphi_r}{\partial r^2}\\
&-\frac{c_1 A_{13}}{r}u_0 - \frac{c_1 A_{14}}{r}\varphi_r - c_1^2 rA_{16}\frac{\partial^2 \varphi_r}{\partial r^2} - c_1^2 rA_{16}\frac{\partial^3 w_0}{\partial r^3} + \frac{c_1^2 A_{16}}{r}\varphi_r\\
&+\frac{c_1^2 A_{16}}{r}\frac{\partial w_0}{\partial r} + rG_{10}\varphi_r - 3c_1 rG_{12}\varphi_r - 3c_1 rG_{12}\frac{\partial w_0}{\partial r} + rG_{10}\frac{\partial w_0}{\partial r} = 0
\end{aligned} \tag{47}$$

where the used coefficients in Eqs. (31)-(47) are defined as

$$A_{1k} = \int_z A_1(z) z^k \, \mathrm{d}z, \qquad k = 0,1,2,...,6 \tag{48}$$

$$B_{1k} = \int_z B_1(z) z^k \, \mathrm{d}z, \qquad k = 0,1,2,...,6 \tag{49}$$

$$G_{1k} = \int_z G(z) z^k \, \mathrm{d}z, \qquad k = 0,1,2,...,6 \tag{50}$$

$$I_k = \int_z \rho(z) z^k \, \mathrm{d}z, \qquad k = 0,1,2,...,6 \tag{51}$$

5. Dimensionless equations

Before solving the governing equations, they are non-dimensionalized. The dimensionless parameters are considered as shown by Eqs. (52)

$$\begin{aligned}
&R = \frac{r}{a}, \quad U = \frac{u_0}{h}, \quad W = \frac{w_0}{h}, \quad \phi_r = \frac{a}{h}\varphi_r, \quad \tau = \frac{t}{a}\sqrt{\frac{A_{10}}{I_0}}\\
&\eta = \frac{h}{a}, \quad \bar{A}_{11} = \frac{A_{11}}{aA_{10}}, \quad \bar{A}_{12} = \frac{A_{12}}{a^2 A_{10}}, \quad \bar{A}_{13} = \frac{c_1 A_{13}}{aA_{10}},\\
&\bar{A}_{14} = \frac{c_1 A_{14}}{a^2 A_{10}}, \quad \bar{A}_{16} = \frac{c_1^2 A_{16}}{a^2 A_{10}}, \quad \bar{G}_{10} = \frac{G_{10}}{A_{10}}, \quad \bar{G}_{12} = \frac{c_1 G_{12}}{A_{10}},\\
&\bar{G}_{14} = \frac{c_1^2 G_{14}}{A_{10}}, \quad \bar{I}_1 = \frac{I_1}{aI_0}, \quad \bar{I}_2 = \frac{I_2}{a^2 I_0}, \quad \bar{I}_3 = \frac{c_1 I_3}{aI_0},\\
&\bar{I}_4 = \frac{c_1 I_4}{a^2 I_0}, \quad \bar{I}_6 = \frac{c_1^2 I_6}{a^2 I_0}, \quad \bar{K}_G = \frac{K_G}{A_{10}}, \quad \bar{K}_W = \frac{K_W a h}{A_{10}},\\
&\bar{C}_d = C_d\sqrt{\frac{A_{10}}{I_0}}
\end{aligned} \tag{52}$$

The dimensionless motion equations are obtained based on CPT as shown by Eqs. (53)-(54)

δU :

$$\begin{aligned}
&R\eta\frac{\partial^2 U}{\partial R^2} + \eta\frac{\partial U}{\partial R} - \frac{1}{R}\eta U - R\eta\bar{A}_{11}\frac{\partial^3 W}{\partial R^3} - \eta\bar{A}_{11}\frac{\partial^2 W}{\partial R^2}\\
&+\frac{1}{R}\eta\bar{A}_{11}\frac{\partial W}{\partial R} - R\eta\frac{\partial^2 U}{\partial \tau^2} = 0
\end{aligned} \tag{53}$$

δW :

$$\begin{aligned}
&R\bar{A}_{11}\eta\frac{\partial^3 U}{\partial R^3} + 2\bar{A}_{11}\eta\frac{\partial^2 U}{\partial R^2} - \frac{1}{R}\bar{A}_{11}\eta\frac{\partial U}{\partial R} + \frac{1}{R^2}\bar{A}_{11}\eta U\\
&-R\eta\bar{A}_{12}\frac{\partial^4 W}{\partial R^4} - 2\eta\bar{A}_{12}\frac{\partial^3 W}{\partial R^3} + \frac{1}{R}\eta\bar{A}_{12}\frac{\partial^2 W}{\partial R^2}\\
&-R\eta\bar{K}_G\frac{\partial^2 W}{\partial R^2} - \frac{1}{R^2}\eta\bar{A}_{12}\frac{\partial W}{\partial R} - \eta\bar{K}_G\frac{\partial W}{\partial R}\\
&+R\bar{K}_W W + R\bar{C}_d\frac{\partial W}{\partial \tau} - R\eta\frac{\partial^2 W}{\partial \tau^2} = 0
\end{aligned} \tag{54}$$

and those of FSDT are given as shown by Eqs. (55)-(57)

δU :

$$\begin{aligned}
&R\eta\frac{\partial^2 U}{\partial R^2} + \eta\frac{\partial U}{\partial R} - \frac{1}{R}\eta U + R\eta\bar{A}_{11}\frac{\partial^2 \phi_r}{\partial R^2} + \eta\bar{A}_{11}\frac{\partial \phi_r}{\partial R} - \frac{1}{R}\eta\bar{A}_{11}\phi_r\\
&-R\eta\frac{\partial^2 U}{\partial \tau^2} - R\eta\bar{I}_1\frac{\partial^2 \phi_r}{\partial \tau^2} = 0
\end{aligned} \tag{55}$$

δW :

$$\begin{aligned}
&R\kappa_f\eta\bar{G}_{10}\frac{\partial^2 W}{\partial R^2} - R\eta\bar{K}_G\frac{\partial^2 W}{\partial R^2} - \eta\bar{K}_G\frac{\partial W}{\partial R} + \kappa_f\eta\bar{G}_{10}\frac{\partial W}{\partial R} + R\bar{K}_W W\\
&+R\kappa_f\eta\bar{G}_{10}\frac{\partial \phi_r}{\partial R} + \kappa_f\eta\bar{G}_{10}\phi_r + R\bar{C}_d\frac{\partial W}{\partial \tau} - R\eta\frac{\partial^2 W}{\partial \tau^2} = 0
\end{aligned} \tag{56}$$

$\delta \phi_r$:

$$\begin{aligned}
&R\eta\bar{A}_{11}\frac{\partial^2 U}{\partial R^2} + \eta\bar{A}_{11}\frac{\partial U}{\partial R} - \frac{1}{R}\eta\bar{A}_{11}U - \kappa_f R\eta\bar{G}_{10}\frac{\partial W}{\partial R} + R\eta\bar{A}_{12}\frac{\partial^2 \phi_r}{\partial R^2}\\
&+\eta\bar{A}_{12}\frac{\partial \phi_r}{\partial R} - \frac{1}{R}\eta\bar{A}_{12}\phi_r - \kappa_f R\eta\bar{G}_{10}\phi_r - R\eta\bar{I}_1\frac{\partial^2 U}{\partial \tau^2}\\
&-R\eta\bar{I}_2\frac{\partial^2 \phi_r}{\partial \tau^2} = 0
\end{aligned} \tag{57}$$

and those corresponding to TSDT thereof are given as shown by Eqs. (58)-(60)

δU :

$$\begin{aligned}
&R\eta\frac{\partial^2 U}{\partial R^2} + \eta\frac{\partial U}{\partial R} - \frac{1}{R}\eta U - R\eta\bar{A}_{13}\frac{\partial^3 W}{\partial R^3} - \eta\bar{A}_{13}\frac{\partial^2 W}{\partial R^2}\\
&+\frac{1}{R}\eta\bar{A}_{13}\frac{\partial W}{\partial R} + R\eta\bar{A}_{11}\frac{\partial^2 \phi_r}{\partial R^2} - R\eta\bar{A}_{13}\frac{\partial^2 \phi_r}{\partial R^2}\\
&-\eta\bar{A}_{13}\frac{\partial \phi_r}{\partial R} + \eta\bar{A}_{11}\frac{\partial \phi_r}{\partial R} - \frac{1}{R}\eta\bar{A}_{11}\phi_r + \frac{1}{R}\eta\bar{A}_{13}\phi_r\\
&-R\eta\frac{\partial^2 U}{\partial \tau^2} + R\eta\bar{I}_3\frac{\partial^3 W}{\partial \tau^2 \partial R} + R\eta\bar{I}_3\frac{\partial^2 \phi_r}{\partial \tau^2} - R\eta\bar{I}_1\frac{\partial^2 \phi_r}{\partial \tau^2} = 0
\end{aligned} \tag{58}$$

δW :

$$\begin{aligned}
&R\eta\bar{A}_{13}\frac{\partial^3 U}{\partial r^3} + 2\eta\bar{A}_{13}\frac{\partial^2 U}{\partial R^2} - \frac{1}{R}\eta\bar{A}_{13}\frac{\partial U}{\partial R} + \frac{1}{R^2}\eta\bar{A}_{13}U - 2\eta\bar{A}_{16}\frac{\partial^3 W}{\partial R^3}\\
&+\eta\bar{G}_{10}\frac{\partial W}{\partial R} + \frac{1}{R}\eta\bar{A}_{16}\frac{\partial^2 W}{\partial R^2} - \frac{1}{R^2}\eta\bar{A}_{16}\frac{\partial W}{\partial R} + 9R\eta\bar{G}_{14}\frac{\partial^2 W}{\partial R^2}\\
&-3R\eta\bar{G}_{12}\frac{\partial^2 W}{\partial R^2} - R\eta\bar{A}_{16}\frac{\partial^4 W}{\partial R^4} - 3R\eta\bar{G}_{12}\frac{\partial^2 W}{\partial R^2} - 3\eta\bar{G}_{12}\frac{\partial W}{\partial R}\\
&+9\eta\bar{G}_{14}\frac{\partial W}{\partial R} + R\eta\bar{G}_{10}\frac{\partial^2 W}{\partial R^2} - R\eta\bar{K}_G\frac{\partial^2 W}{\partial R^2} - \eta\bar{K}_G\frac{\partial W}{\partial R} + R\bar{K}_W W\\
&-3\eta\bar{G}_{12}\frac{\partial W}{\partial R} - 2\eta\bar{A}_{16}\frac{\partial^2 \phi_r}{\partial R^2} + R\eta\bar{A}_{14}\frac{\partial^3 \phi_r}{\partial R^3} - \frac{1}{R^2}\eta\bar{A}_{16}\phi_r + \eta\bar{G}_{10}\phi_r\\
&+9R\eta\bar{G}_{14}\frac{\partial \phi_r}{\partial R} + \frac{1}{R}\eta\bar{A}_{16}\frac{\partial \phi_r}{\partial R} - \frac{1}{R}\eta\bar{A}_{14}\frac{\partial \phi_r}{\partial R} + \frac{1}{R^2}\eta\bar{A}_{14}\phi_r\\
&-3R\eta\bar{G}_{12}\frac{\partial \phi_r}{\partial R} + 9\eta\bar{G}_{14}\phi_r - 3R\eta\bar{G}_{12}\frac{\partial \phi_r}{\partial R} + R\eta\bar{G}_{10}\frac{\partial \phi_r}{\partial R} - 3\eta\bar{G}_{12}\phi_r\\
&+2\eta\bar{A}_{14}\frac{\partial^2 \phi_r}{\partial R^2} - 3\eta\bar{G}_{12}\phi_r - R\eta\bar{A}_{16}\frac{\partial^3 \phi_r}{\partial R^3} + R\bar{C}_d\frac{\partial W}{\partial \tau} - R\eta\bar{I}_3\frac{\partial^3 U}{\partial \tau^2 \partial R}\\
&-\eta\bar{I}_3\frac{\partial^2 U}{\partial \tau^2} + R\eta\bar{I}_6\frac{\partial^4 W}{\partial \tau^2 \partial R^2} + \eta\bar{I}_6\frac{\partial^3 W}{\partial \tau^2 \partial R} - R\eta\frac{\partial^2 W}{\partial \tau^2} + R\eta\bar{I}_6\frac{\partial^3 \phi_r}{\partial \tau^2 \partial R}\\
&-R\eta\bar{I}_4\frac{\partial^3 \phi_r}{\partial \tau^2 \partial R} - \eta\bar{I}_4\frac{\partial^2 \phi_r}{\partial \tau^2} + \eta\bar{I}_6\frac{\partial^2 \phi_r}{\partial \tau^2} = 0
\end{aligned} \tag{59}$$

$\delta \phi_r$: (60)

$$
\begin{aligned}
&R\eta\bar{A}_{11}\frac{\partial^2 U}{\partial R^2}-R\eta\bar{A}_{13}\frac{\partial^2 U}{\partial R^2}-\eta\bar{A}_{13}\frac{\partial U}{\partial R}+\eta\bar{A}_{11}\frac{\partial U}{\partial R}-\frac{1}{R}\eta\bar{A}_{11}U\\
&+\frac{1}{R}\eta\bar{A}_{13}U+R\eta\bar{A}_{16}\frac{\partial^3 W}{\partial R^3}-R\eta\bar{A}_{14}\frac{\partial^3 W}{\partial R^3}-\eta\bar{A}_{14}\frac{\partial^2 W}{\partial R^2}\\
&+\eta\bar{A}_{16}\frac{\partial^2 W}{\partial R^2}-9R\eta\bar{G}_{14}\frac{\partial W}{\partial R}-\frac{1}{R}\eta\bar{A}_{16}\frac{\partial W}{\partial R}+3R\eta\bar{G}_{12}\frac{\partial W}{\partial R}\\
&+\frac{1}{R}\eta\bar{A}_{14}\frac{\partial W}{\partial R}-R\eta\bar{G}_{10}\frac{\partial W}{\partial R}+3R\eta\bar{G}_{12}\frac{\partial W}{\partial R}+R\eta\bar{A}_{12}\frac{\partial^2\phi_r}{\partial R^2}\\
&+R\eta\bar{A}_{16}\frac{\partial^2\phi_r}{\partial R^2}-R\eta\bar{A}_{14}\frac{\partial^2\phi_r}{\partial R^2}-R\eta\bar{A}_{14}\frac{\partial^2\phi_r}{\partial R^2}-\eta\bar{A}_{14}\frac{\partial\phi_r}{\partial R}\\
&+\eta\bar{A}_{16}\frac{\partial\phi_r}{\partial R}-\eta\bar{A}_{14}\frac{\partial\phi_r}{\partial R}+\eta\bar{A}_{12}\frac{\partial\phi_r}{\partial R}+3R\eta\bar{G}_{12}\phi_r-R\eta\bar{G}_{10}\phi_r\\
&+\frac{1}{R}\eta\bar{A}_{14}\phi_r+3R\eta\bar{G}_{12}\phi_r-9R\eta\bar{G}_{14}\phi_r-\frac{1}{R}\eta\bar{A}_{16}\phi_r+\frac{1}{R}\eta\bar{A}_{14}\phi_r\\
&-\frac{1}{R}\eta\bar{A}_{12}\phi_r-R\eta\bar{I}_1\frac{\partial^2 U}{\partial\tau^2}+R\eta\bar{I}_3\frac{\partial^2 U}{\partial\tau^2}-R\eta\bar{I}_6\frac{\partial^3 W}{\partial\tau^2\partial R}\\
&+R\eta\bar{I}_4\frac{\partial^3 W}{\partial\tau^2\partial R}-R\eta\bar{I}_2\frac{\partial^2\phi_r}{\partial\tau^2}-R\eta\bar{I}_6\frac{\partial^2\phi_r}{\partial\tau^2}+2R\eta\bar{I}_4\frac{\partial^2\phi_r}{\partial\tau^2}=0
\end{aligned}
$$

6. Solution procedure

6.1 GDQM

For numerical approximation of the solution of the dimensionless governing differential motion Eqs. (53)-(60), they must be converted into difference equations. In the current manuscript the equations are discretized by the application of GDQ method. According to GDQ method presented by Ref.s (Hosseini-Hashemi and Khorami 2011, Zong *et al*. 2009), the *m-th* order derivative of a function at a grid point, namely $F^{(m)}(x_i)$ or $d^mF(x_i)/dx^{(m)}$, is approximated by a linear combination of the function values in whole grid points as shown by Eq. (61) within which the weighting coefficients $C_{ij}^{(m)}$ are calculated using Lagrange's interpolating polynomials (Liew *et al*. 1996)

$$\frac{d^m F}{dx^m}(x_i)=\sum_{n=1}^{N}c_{in}^{(m)}F(x_n),\qquad 1\le i,\ n\le N,\ m<N \tag{61}$$

The number of the entire grid points, namely *N*, is so chosen that the GDQ method is guaranteed against instability.

Eqs. (62)-(63) show the well-known interpolation of function $F(x)$ with Lagrange's interpolating polynomials, and its *m-th* order derivative.

$$F(x)\cong P_{N-1}(x)=\sum_{n=1}^{N}F(x_n)\,L_n(x), \tag{62}$$

$$F^{(m)}(x_i)\cong P_{N-1}^{(m)}(x_i)=\sum_{n=1}^{N}F(x_n)\,L_n^{(m)}(x_i)\equiv\sum_{n=1}^{N}c_{in}^{(m)}F(x_n) \tag{63}$$

where

$$
\begin{aligned}
L_n(x)&=\frac{L(x)}{(x-x_n)L^{(1)}(x_n)},\\
L(x)&=\prod_{n=1}^{N}(x-x_n)
\end{aligned} \tag{64}
$$

The first derivatives of $L(x)$, i.e. Eq. (65), in the *i-th* grid point is given by Eq. (53)

$$L^{(1)}(x_i)=\prod_{\substack{n=1\\ n\ne i}}^{N}(x_i-x_n) \tag{65}$$

By mathematical simplification, the GDQM weighting coefficients are achieved as shown by Eqs. (66)-(69) can be found (Liew *et al*. 1996)

$$L_n^{(1)}(x_i)=c_{in}^{(1)}=\frac{L^{(1)}(x_i)}{(x_i-x_n)L^{(1)}(x_n)},\qquad i\ne n \tag{66}$$

$$c_{in}^{(m)}=m\left[c_{ii}^{(m-1)}c_{in}^{(1)}-\frac{c_{in}^{(m-1)}}{(x_i-x_n)}\right],\ i\ne n,\ 2\le m<N \tag{67}$$

$$c_{ii}^{(1)}=-\sum_{\substack{n=1\\ n\ne i}}^{N}c_{in}^{(1)}, \tag{68}$$

$$c_{ii}^{(m)}=-\sum_{\substack{n=1\\ n\ne i}}^{N}c_{in}^{(m)},\quad 2\le m<N \tag{69}$$

The distribution of the grid points in the dimensionless domain of the differential equations has a considerable influence upon the stability of the GDQM for solving the discrete singular equations. Shu and Richards (1992) has proposed a method for selecting the entire grid points. The set of the dimensionless grid points with uniform and with *Chebyshev-Gauss-Lobatto* distributions are respectively generated by Eqs. (70)-(71). Bert and Malik (1996) have prescribed *Chebyshev-Gauss-Lobatto* grid points for computational structural mechanics.

$$R_n=\frac{n-1}{N-1},\qquad 1\le n\le N \tag{70}$$

$$R_n=\left\{1-\cos\left[\pi(n-1)/(N-1)\right]\right\}/2,\qquad 1\le n\le N \tag{71}$$

Since the current manuscript deals with singular differential equations, the GDQM numerical performance caused by *Chebyshev-Gauss-Lobatto* distribution has appeared much better than that caused by uniform one.

6.2 Assembling

The motion, continuity and boundary equations construct the set of ordinary homogeneous differential equations as shown by Eq. (72)

$$\left(\begin{bmatrix}K_{dd} & K_{db}\\ K_{bd} & K_{bb}\end{bmatrix}+i\begin{bmatrix}C_{dd} & C_{db}\\ C_{bd} & C_{bb}\end{bmatrix}\omega-\begin{bmatrix}M_{dd} & M_{db}\\ M_{bd} & M_{bb}\end{bmatrix}\omega^2\right)\begin{Bmatrix}d\\ b\end{Bmatrix}=0 \tag{72}$$

where *d* and *b* denote the displacements of the inner and boundary points, respectively. Solving the above eigenvalue problem, leads to obtain the natural frequencies of the plate.

7. Numerical results and discussion

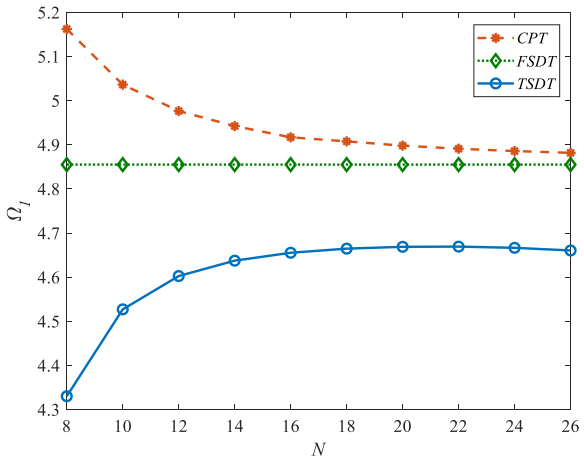

(a)

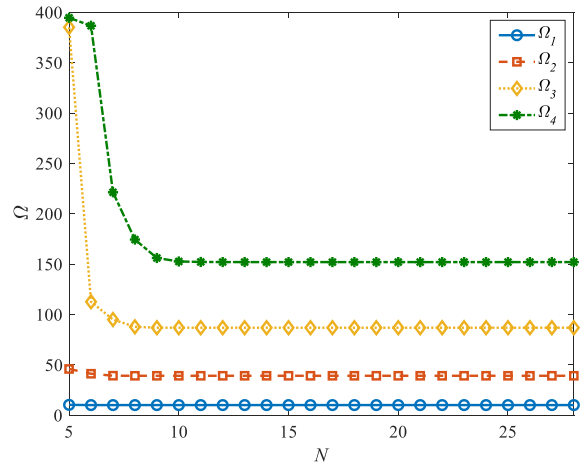

(b)

Fig. 2 Convergence of the results for a) first dimensionless frequency based on CP, FSD and TSD theories; b) first four frequencies based on FSDT. (Symmetric dist.)

In this section, the results for the free vibration analysis of the considering plate are presented. Firstly, the convergence of the GDQ method is investigated, then by comparing the present study results with previous ones, the reliability of them is examined and after that the results of the current research are expressed.

7.1 Convergence

As stated in the previous section, choosing the right number of grid points plays an important role in stability and convergence of the obtained results via GDQM. So, Fig. 2 shows the effect of grid points number on the results. Fig. 2(a) indicates the mentioned effect for the first natural frequency obtained by CPT, FSDT and TSDT. It is seen that the FSDT results are converged to a specific value with fewer number of grid points in comparison those of CPT and TSDT. Also, it can be found that by choosing 20 grid points, the results for three mentioned theories are converged to their final values. Fig. 2(b) considers the convergence of FSDT results for first four frequencies. It is seen that the first frequency is converged sooner than the higher modes frequencies. So, the rapid convergence which is one of the highlight features of the GDQM is examined and it is seen that with few number of points the results are converged.

Table 1 Comparing the results of first four dimensionless frequencies with previous studies

B.C	Ref.		Ω_1	Ω_2	Ω_3	Ω_4
C	Azimi (1998)		10.216	39.771	89.103	-
	Wu *et al.* (2002)		10.216	39.771	89.104	158.184
	Lal and Ahlawat (2015)		10.2158	39.7711	89.1041	-
	Wang *et al.* (2001)		10.197	39.418	-	-
	Leissa (1969)		10.2158	39.771	89.104	158.1842
	Present	CPT	10.30963	40.13858	89.93241	159.6635
		FSDT	10.27701	39.71432	87.99016	153.9437
		TSDT	10.01009	39.24168	87.28626	153.2252
S	Azimi, 1998		4.935	29.720	74.156	-
	Wu *et al.* (2002)		4.935	29.720	74.156	138.318
	Lal and Ahlawat (2015)		4.9351	29.7200	74.1561	-
	Leissa (1969)		4.977	29.76	74.20	138.34
	Present	CPT	4.981802	30.05704	74.99636	139.8847
		FSDT	4.97552	29.81088	73.71986	135.7879
		TSDT	4.70749	29.26333	72.98983	134.8865

7.2 Validation

By substituting e_1 and B with zero, the porosity and Skempton's number are neglected and the mathematical model of the porous FG circular plate is reduced into that of isotropic one. The lowest four dimensionless natural frequencies of such a plate with clamped and simple supports boundary conditions have been computed based on CP, FSD and TSD theories and compared with literature in Table 1 (Azimi 1988, Lal and Ahlawat 2015, Leissa 1969, Wang *et al.* 2001, Wu *et al.* 2002). The lowest dimensionless natural frequency is analytically given by $\Omega = \omega a^2 \sqrt{\rho h / D}$ within which the plate flexural rigidity is computed from $D=Eh^3/12(1-\nu^2)$. The plate material is steel possessing modulus of elasticity E, Poisson's ratio and density equal to 200 GPa, 0.3 and 7800 kg/m^3, respectively. It is seen that the results are in excellent agreement with previous ones and the little difference is due to different theories were used to analyze the structure. So, the reliability if the equations and solution method is also validated and in the following, the present study with considering different material, foundation and aspect ratio parameters are investigated.

7.3 Parametric study

Now, effect of different parameters on the natural frequencies and mode shapes of the under considerations plate are studied. It should be noted that the plate's radius and thickness are considered to be 0.6 m and 0.02 m, respectively and it's Young's elasticity modulus and density

Table 2 Effect of Skempton coefficient, porosity and boundary conditions on the first dimensionless frequency based on CP, FSD and TSD theories for non-symmetric porosity distribution

			e_1			
B	B.C		0.0	0.2	0.4	0.6
0.0	S	CPT	4.8559	4.7244	4.5843	4.4359
		FSDT	4.8278	4.6970	4.5578	4.4105
		TSDT	4.6540	4.5264	4.3902	4.2443
	C	CPT	10.1573	9.8639	9.4933	8.9790
		FSDT	10.1271	9.8343	9.4649	8.9531
		TSDT	9.8732	9.5860	9.2246	8.7267
0.3	S	CPT	-	4.7872	4.6959	4.5793
		FSDT	-	4.7594	4.6686	4.5530
		TSDT	-	4.5846	4.4934	4.3761
	C	CPT	-	9.9587	9.6753	9.2386
		FSDT	-	9.9283	9.6455	9.2106
		TSDT	-	9.6749	9.3958	8.9706
0.5	S	CPT	-	4.8281	4.7672	4.6697
		FSDT	-	4.8000	4.7395	4.6427
		TSDT	-	4.6228	4.5595	4.4594
	C	CPT	-	10.0203	9.7908	9.3993
		FSDT	-	9.9894	9.7599	9.3700
		TSDT	-	9.7329	9.5039	9.1212

Table 3 Effect of Skempton coefficient, porosity and boundary conditions on the first dimensionless frequency based on CP, FSD and TSD theories for symmetric porosity distribution

			e_1			
B	B.C		0.0	0.2	0.4	0.6
0.0	S	CPT	4.8559	4.8430	4.8534	4.9108
		FSDT	4.8278	4.8147	4.8248	4.8814
		TSDT	4.6540	4.6335	4.6319	4.6678
	C	CPT	10.1573	10.1301	10.1520	10.2720
		FSDT	10.1271	10.0982	10.1177	10.2339
		TSDT	9.8732	9.8330	9.8341	9.9178
0.3	S	CPT	-	4.8837	4.9307	5.0204
		FSDT	-	4.8552	4.9015	4.9902
		TSDT	-	4.6685	4.6984	4.7629
	C	CPT	-	10.1883	10.2624	10.4288
		FSDT	-	10.1559	10.2270	10.3890
		TSDT	-	9.8870	9.9356	10.0602
0.5	S	CPT	-	4.9106	4.9809	5.0908
		FSDT	-	4.8818	4.9514	5.0602
		TSDT	-	4.6914	4.7421	4.8246
	C	CPT	-	10.2267	10.3345	10.5303
		FSDT	-	10.1939	10.2984	10.4895
		TSDT	-	9.9225	10.0019	10.1523

respectively are as 60 GPa and 2700 kg/m^3. Also, the value of Poisson's ratio is 0.25.

The first dimensionless natural frequencies of clamped and simply supported circular porous FG plate are computed for CP, FSD and TSD theories and are shown in Tables 2-4 for the assigned values 0.0, 0.3 and 0.5 for Skempton parameter and non-symmetric, symmetric and monotonic pore distributions. According to these tables, the increase of pore compressibility or Skempton parameter, increases the natural frequency due to increasing the stiffness of the plate compare to its density.

Considering Table 2, due to the increase of porosity in a circular plate with non-symmetrical pores distribution, the first natural frequency decreases in both clamped and simple boundary conditions. These behaviors are due to the fact that in the plate, both mass and stiffness decrease due to porosity increase, but the rate of decrease of stiffness is more than that of mass. Since the frequency is proportional to the square root of the ratio of stiffness to mass, the natural frequency decreases. This is in compliance with References (Chen *et al.* 2016, Leclaire *et al.* 2001, Theodorakopoulos and Beskos 1994).

Considering Table 3, due to the increase of porosity in a circular plate with symmetrical pores distribution, the first natural frequency increases unlike the non-symmetric distribution. Its reason is due to stiffness to mass ratio variations.

Considering Table 4, it is found that the plate's natural frequency has a similar manner to non-symmetric pores distribution for monotonic distribution.

Table 4 Effect of Skempton coefficient, porosity and boundary conditions on the first dimensionless frequency based on CP, FSD and TSD theories for monotonous porosity distribution

			e_1			
B	B.C		0.0	0.2	0.4	0.6
0.0	S	CPT	4.8559	4.6899	4.4940	4.2500
		FSDT	4.8278	4.6627	4.4680	4.2254
		TSDT	4.6540	4.4948	4.3071	4.0732
	C	CPT	10.1573	9.8100	9.4003	8.8899
		FSDT	10.1271	9.7808	9.3723	8.8634
		TSDT	9.8732	9.5357	9.1375	8.6413
0.3	S	CPT	-	4.7636	4.6368	4.4566
		FSDT	-	4.7359	4.6099	4.4306
		TSDT	-	4.5646	4.4423	4.2686
	C	CPT	-	9.9152	9.6049	9.1869
		FSDT	-	9.8851	9.5752	9.1579
		TSDT	-	9.6346	9.3299	8.9205
0.5	S	CPT	-	4.8116	4.7280	4.5856
		FSDT	-	4.7837	4.7005	4.5589
		TSDT	-	4.6101	4.5284	4.3904
	C	CPT	-	9.9842	9.7371	9.3754
		FSDT	-	9.9535	9.7062	9.3447
		TSDT	-	9.6995	9.4539	9.0972

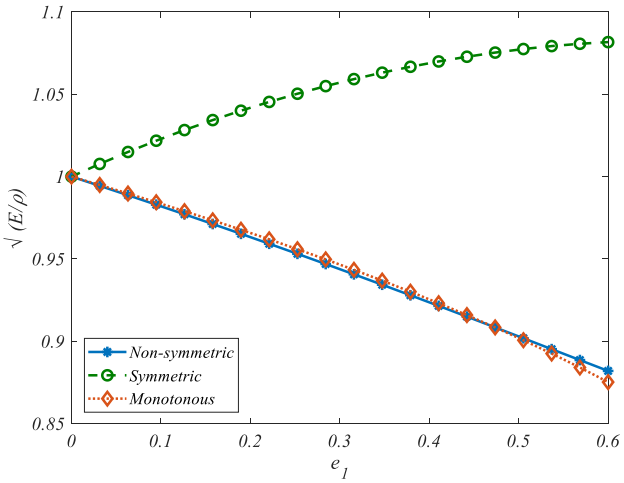

Fig. 3 Variations of stiffness to density ratio respect to porosity coefficient

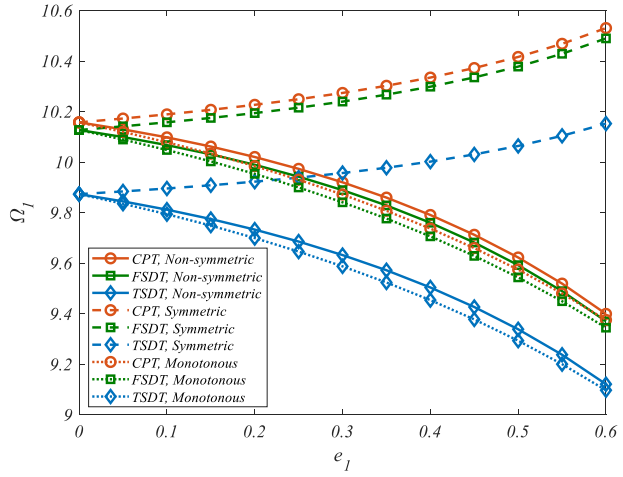

(a)

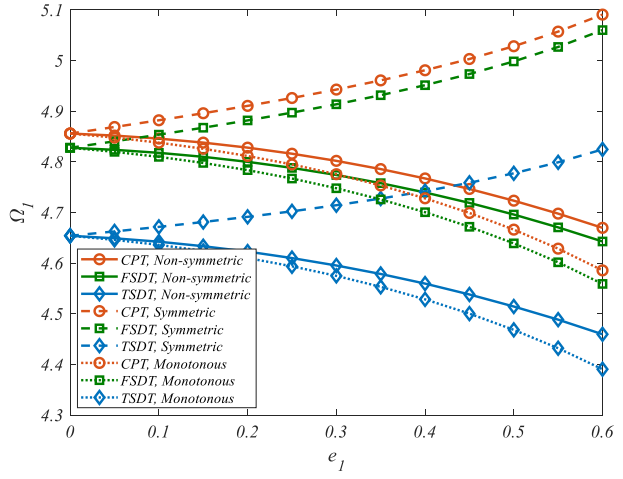

(b)

Fig. 4 Effect of porosity increasing, different theories and porosity distributions on first natural frequency of (a) clamped; (b) simple supports circular plate

Square root of the ratio of stiffness to mass is plotted respect to the porosity variations in Fig. 3 and it confirms

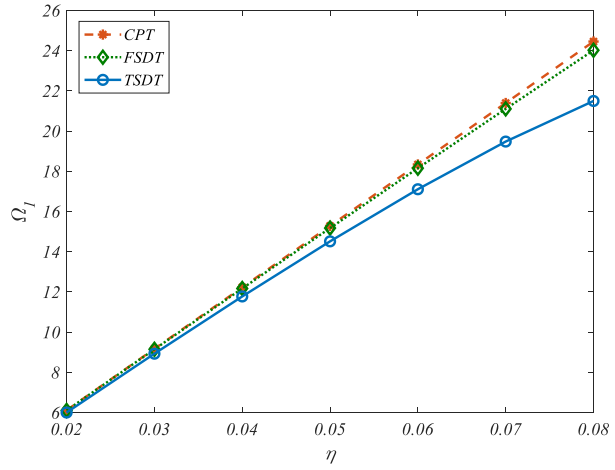

(a)

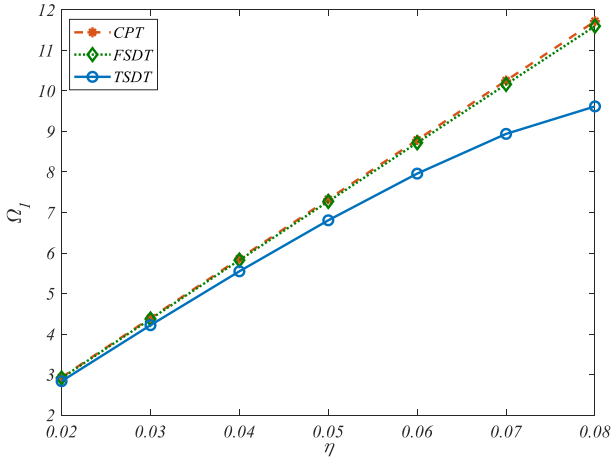

(b)

Fig. 5 Effect of dimensionless thickness on the first dimensionless frequency of (a) clamped; (b) simple supports circular plate based on CP, FSD and TSD theories

the previous statements.

Figs. 4(a)-(b) show the effect of pores distribution, porosity coefficient and compare the results of three used theories. Fig. 4(a) shows the first dimensionless natural frequency variations versus porosity coefficient for clamped plate and Fig. 4(b) shows the same thing but for simple supports circular plate. These figures confirmed the findings of Tables 2-4 and also indicate that by accounting the shear deformations effect and also by increasing the order of used theory, the results become more accurate. In other words, the results of TSDT are the least ones in comparison to CPT and FSDT. Since the TSDT accounts the shear deformations using a third order function, it is more accurate than two other theories. Also, between CPT and FSDT, it is seen that the results of CPT are more than FSDT. This happens for all of the following results.

As shown by Figs. 5(a)-(b), increase of dimensionless thickness increases the first natural frequency of a circular plate for symmetric pores distribution. In clamped boundary conditions, the slope of increase of the frequency is greater in comparison with the slope in simple boundary conditions. As stated before, it is also obvious that TSDT

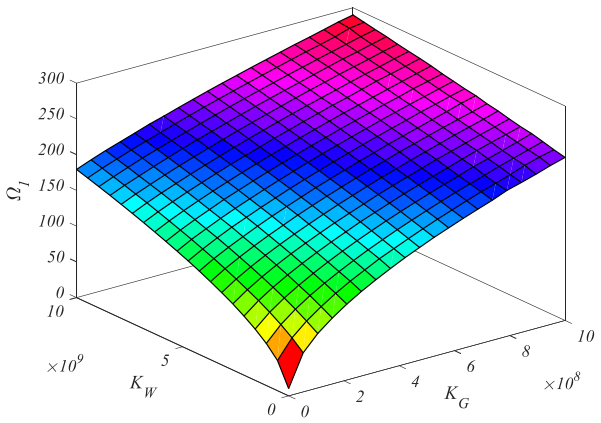

Fig. 6 Effect of spring and shear layer constants on first natural frequency of the plate

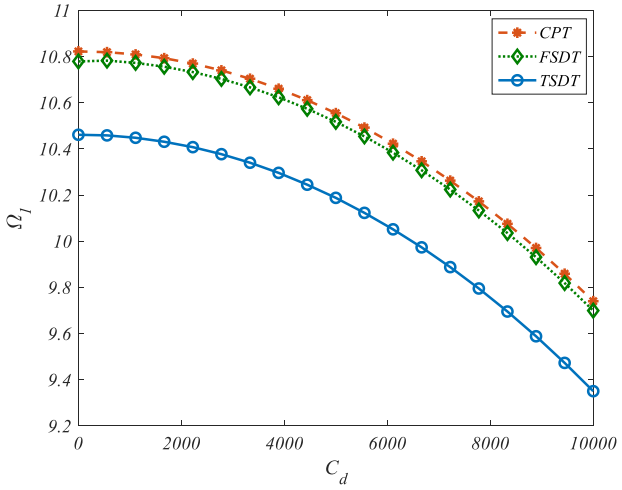

Fig. 7 Effect of damping constant on frequency of the plate

has the minimum values of the results than those of CPT and FSDT. As the plate's thickness becomes less, in another word for thin plates, the difference between results of three mentioned theories are negligible but as the plate becomes thicker, the difference becomes more, too. It can be concluded due to more complex equations and more CPU time usage for solving the TSDT equations, it is recommended that for thin plates, CPT be used for describing the displacement components, FSDT for moderately thick and TSDT for thick plates.

Figs. 6-8 depict effect of visco-elastic foundation constants on the vibration of the plate for symmetric porosity distribution. Fig. 6 shows the effect of spring and shear layer constants simultaneously. As the mentioned constants increase, the stiffness of the structure enhances and its vibration reduces, so its natural frequency increases. Comparing spring and shear layer constants effect, it is seen spring constant has more effect on the results.

Fig. 7 shows the damping constant variations on the results. As the damping constants enhances, its viscosity increases and effect of dampers, reduces. It will caused a reducing in natural frequency and leads to increasing the vibrations of the plate.

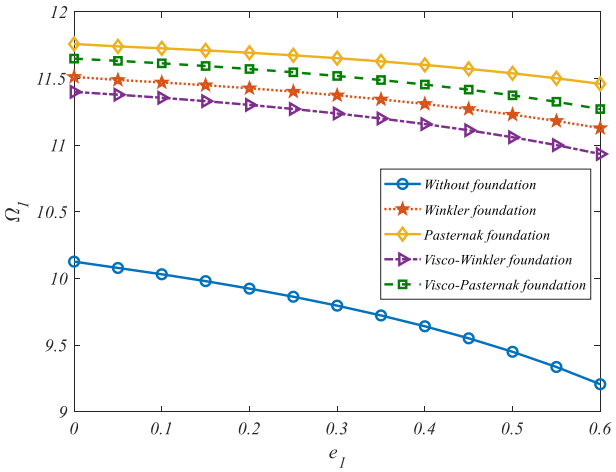

Fig. 8 Comparison of different types of elastic foundation and their effect on natural frequency

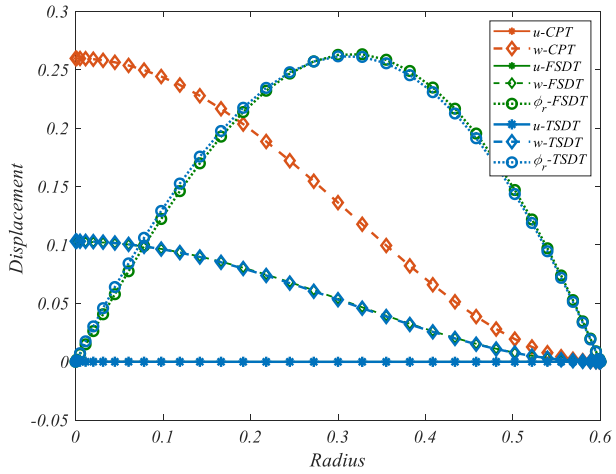

(a)

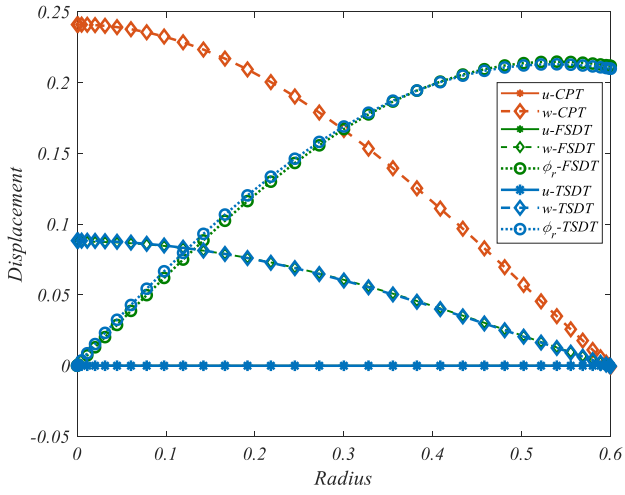

(b)

Fig. 9 Associated to first frequency mode shapes based on CP, FSD and TSD theories for (a) clamped; (b) simple supports plate

Comparing different types of elastic foundation and their influence on the vibrational behavior of the plate is

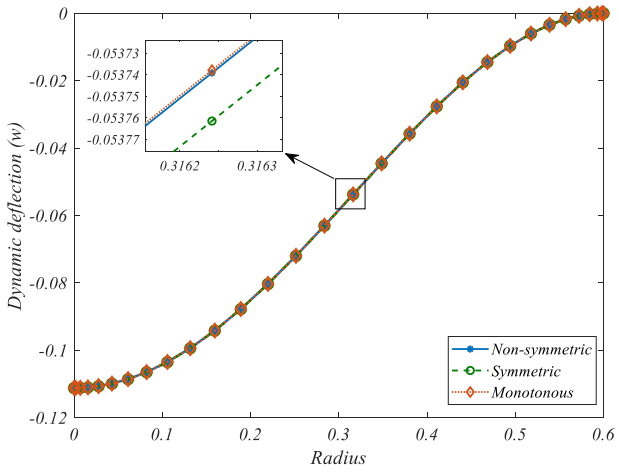

Fig. 10 Effect of porosity distributions on deflection of the plate along the radius

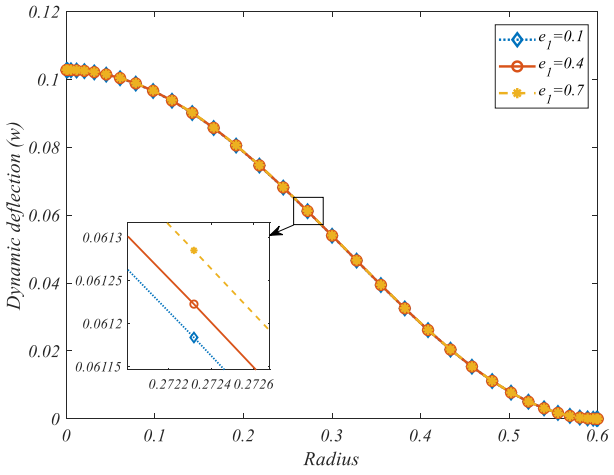

Fig. 11 Effect of porosity increasing on deflection of the plate along the radius

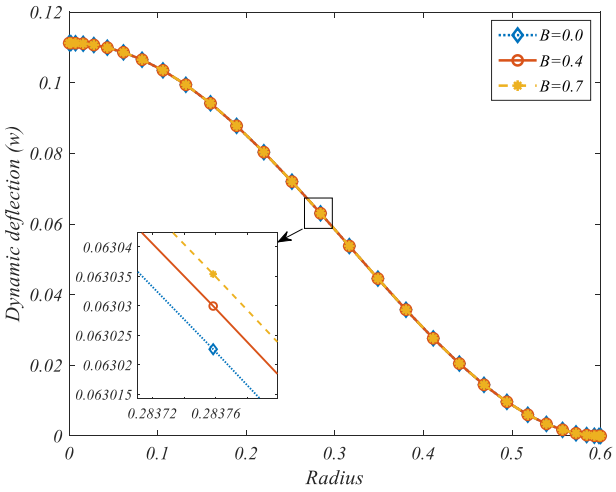

Fig. 12 Effect of Skempton coefficient variations on deflection of the plate along the radius

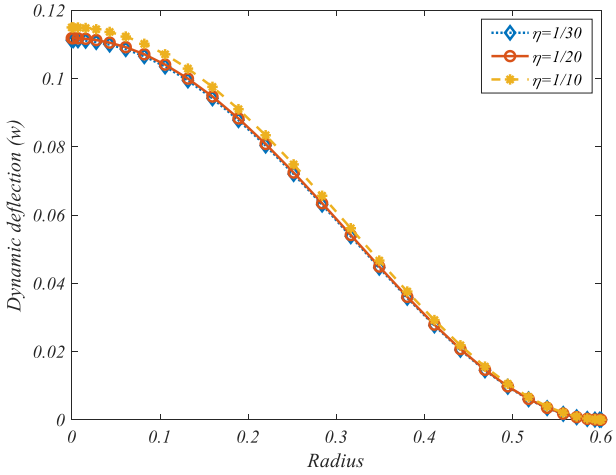

Fig. 13 Effect of dimensionless thickness on deflection of the plate along the radius

considered in Fig. 8. It is seen if the elastic foundation will be removed from the structure, its frequency decreases and by adding different kinds of elastic substrate, it will be increased. Also, among the different types of elastic foundation, it is concluded that Pasternak and visco-Winkler have the maximum and minimum values of natural frequencies, respectively. As it was found in Fig. 8, generally adding the damper, increases the vibration of the structure.

Figs. 9-13 are considered effect of the previous parameters on the mode shapes of the vibration first mode of the plate. Figs. 9(a)-(b) are plotted the displacement components of the plate based on CP, FSD and TSD theories along the radius of the plate for non-symmetric pores distribution. The physical meaning of boundary conditions can be seen in these figures. Fig. 9(a) is for clamped plate and Fig. 9(b) is for simple supports one. Also, the distribution of grid points according to *Chebyshev-Gauss-Lobatto* is clearly seen in these figures. Based on the mentioned points distribution, number of points near the boundaries are more than other areas. Noted that *u* displacement is not zero but it is negligible compare to other components.

Dynamic transverse displacement of the clamped plate is plotted in Fig. 10 for different porosity distributions for the first mode of vibration based on FSDT. It is seen the symmetric and monotonic distributions have the most and the least dynamic deflection, respectively.

Also, effect of porosity increasing on the dynamic deflection of the plate along its radius is shown in Fig. 11. As the porosity increases, the plates dynamic deflection increases and also it vibrates more.

Fig. 12 illustrates effect of Skempton parameter on the dynamic transverse displacement of the structure. It is found that enhancing *B*, leads the deflection to increase.

Fig. 13 depicts effect of thickness of the plate on *w*. It is seen as the plate becomes thicker, its dynamic displacement raises.

8. Conclusions

Using GDQM the governing differential equations and

boundary conditions of saturated porous circular plate which have been derived based on CP, FSD and TSD theories, have been converted into discrete algebraic ones. The effect of material, foundation and geometric parameters on the natural frequencies and mode shapes has been analyzed and the following items are concluded:

• Employing GDQM to solve the governing differential equations, caused a rapid convergence and high accurate results in comparison to previous studies.

• By neglecting the porosity and Skempton parameters, the mathematical model and results are converted into those of an isotropic circular plate.

• Increase of compressibility of the fluids within the pores increases the natural frequency and the dynamic deflection of the plate.

• Increase of porosity from zero makes the natural frequency of simply supported and clamped circular plates decreases for non-symmetric and monotonous pores distributions, but increases for symmetric distribution. This is due to stiffness to mass ratio variations for each types of porosity distribution. Also, the symmetric distribution has the most dynamic deflection and monotonous has the least.

• Enhancing of dimensionless thickness, increases the first natural frequency and dynamic deflection of the circular plate. For clamped supports it increases with a greater slope than that of the simply supported one.

• Comparing the results of CPT, FSDT and TSDT it is found that the TSDT ones have the least values and CPT results have the most. Also, as the plate becomes thicker, TSDT is a better choice for its analysis. While CPT and FSDT are recommended to analyze the thin and moderately thick plates, respectively.

• Since adding elastic foundation generally increases the plate's stiffness, so the natural frequency of the plate increases, too.

• Although increasing the spring and shear layer constants, increases the frequency, but enhancing the damping constant, reduces the frequency and vibrates plate more.

• Comparing different kinds of elastic foundation, it is found that Pasternak and visco-Winkler foundations have the maximum and minimum values of frequency, respectively.

References

Allahverdizadeh, A., Naei, M.H. and Nikkhah Bahrami, M. (2008), "Nonlinear free and forced vibration analysis of thin circular functionally graded plates", *J. Sound Vibr.*, **310**(4-5), 966-984.

Amir, S. (2016), "Orthotropic patterns of visco-Pasternak foundation in nonlocal vibration of orthotropic graphene sheet under thermo-magnetic fields based on new first-order shear deformation theory", *J. Mater. Des. Appl.*, **233**(2), 197-208.

Amir, S., Bidgoli, E.M.R. and Arshid, E. (2018a), "Size-dependent vibration analysis of a three-layered porous rectangular nano plate with piezo-electromagnetic face sheets subjected to pre loads based on SSDT", *Mech. Adv. Mater. Struct.*, 1-15.

Amir, S., Khorasani, M. and BabaAkbar-Zarei, H. (2018b), "Buckling analysis of nanocomposite sandwich plates with piezoelectric face sheets based on flexoelectricity and first-order shear deformation theory", *J. Sandw. Struct. Mater.*, 109963621879538.

Arefi, M. and Zenkour, A.M. (2017), "Thermo-electro-magneto-mechanical bending behavior of size-dependent sandwich piezomagnetic nanoplates", *Mech. Res. Commun.*, **84**, 27-42.

Arshid, E. and Khorshidvand, A.R. (2017), "Flexural vibrations analysis of saturated porous circular plates using differential quadrature method", *Iran. J. Mech. Eng. Trans. ISME*, **19**(1), 78-100.

Arshid, E. and Khorshidvand, A.R. (2018), "Free vibration analysis of saturated porous FG circular plates integrated with piezoelectric actuators via differential quadrature method", *Thin-Wall. Struct.*, **125**, 220-233.

Azimi, S. (1988), "Free vibration of circular plates with elastic edge supports using the receptance method", *J. Sound Vibr.*, **120**(1), 19-35.

Belmahi, S., Zidour, M., Meradjah, M., Bensattalah, T. and Dihaj, A. (2018), "Analysis of boundary conditions effects on vibration of nanobeam in a polymeric matrix", *Struct. Eng. Mech.*, **67**(5), 517-525.

Bennoun, M., Houari, M.S.A. and Tounsi, A. (2016), "A novel five-variable refined plate theory for vibration analysis of functionally graded sandwich plates", *Mech. Adv. Mater. Struct.*, **23**(4), 423-431.

Bert, C.H.W., Jang, S.K. and Striz, A.G. (1989), "Nonlinear bending analysis of orthotropic rectangular plates by the method of differential quadrature", *Comput. Mech.*, **5**(2-3), 217-226.

Bert, C.W. and Malik, M. (1996), "Differential quadrature method in computational mechanics: A review", *Appl. Mech. Rev.*, **49**(1), 1-28.

Biot, M.A. (1964), "Theory of buckling of a porous slab and its thermoelastic analogy", *J. Appl. Mech.*, **31**(2), 194-198.

Brush, D.O., Almroth, B.O. and Hutchinson, J.W. (1975), "Buckling of bars, plates, and shells", *J. Appl. Mech.*, **42**, 911.

Camier, C., Touzé, C. and Thomas, O. (2009), "Non-linear vibrations of imperfect free-edge circular plates and shells", *Eur. J. Mech.-A/Sol.*, **28**(3), 500-515.

Chen, C.S. (2005), "Nonlinear vibration of a shear deformable functionally graded plate", *Compos. Struct.*, **68**(3), 295-302.

Chen, D., Yang, J. and Kitipornchai, S. (2016), "Free and forced vibrations of shear deformable functionally graded porous beams", *Int. J. Mech. Sci.*, **108**, 14-22.

Civalek, Ö. (2004), "Application of differential quadrature (DQ) and harmonic differential quadrature (HDQ) for buckling analysis of thin isotropic plates and elastic columns", *Eng. Struct.*, **26**(2), 171-186.

Cong, P.H., Chien, T.M., Khoa, N.D. and Duc, N.D. (2018), "Nonlinear thermomechanical buckling and post-buckling response of porous FGM plates using Reddy's HSDT", *Aerosp. Sci. Technol.*, **77**, 419-428.

Decha-Umphai, K. and Mei, C. (1986), "Finite element method for non-linear forced vibrations of circular plates", *Int. J. Numer. Meth. Eng.*, **23**(9), 1715-1726.

Detournay, E. and Cheng, A.H.D. (1993), "Fundamentals of poroelasticity", *Analy. Des. Meth.*, 113-171.

Duc, N.D. (2013), "Nonlinear dynamic response of imperfect eccentrically stiffened FGM double curved shallow shells on elastic foundation", *Compos. Struct.*, **99**, 88-96.

Duc, N.D. (2014), *Nonlinear Static and Dynamic Stability of Functionally Graded Plates and Shells*, Vietnam National University Press.

Duc, N.D. (2016), "Nonlinear thermal dynamic analysis of eccentrically stiffened S-FGM circular cylindrical shells surrounded on elastic foundations using the Reddy's third-order shear deformation shell theory", *Eur. J. Mech., A/Sol.*, **58**, 10-30.

Duc, N.D. (2018), "Nonlinear thermo-electro-mechanical dynamic

response of shear deformable piezoelectric sigmoid functionally graded sandwich circular cylindrical shells on elastic foundations", *J. Sandw. Struct. Mater.*, **20**(3), 351-378.

Duc, N.D. and Ha, N. (2011), "The bending analysis of thin composite plate under steady temperature field", *J. Sci. Math.-Phys.*, **27**(2), 77-83.

Duc, N.D. and Quan, T.Q. (2015), "Nonlinear dynamic analysis of imperfect functionally graded material double curved thin shallow shells with temperature-dependent properties on elastic foundation", *J. Vibr. Contr.*, **21**(7), 1340-1362.

Duc, N.D., Cong, P.H., Tuan, N.D., Tran, P. and Thanh, N.V. (2017), "Thermal and mechanical stability of functionally graded carbon nanotubes (FG CNT)-reinforced composite truncated conical shells surrounded by the elastic foundations", *Thin-Wall. Struct.*, **115**, 300-310.

Duc, N.D., Seung-Eock, K. and Chan, D.Q. (2018), "Thermal buckling analysis of FGM sandwich truncated conical shells reinforced by FGM stiffeners resting on elastic foundations using FSDT", *J. Therm. Stress.*, **41**(3), 331-365.

Duc, N., Dinh Nguyen, P. and Dinh Khoa, N. (2017), "Nonlinear dynamic analysis and vibration of eccentrically stiffened S-FGM elliptical cylindrical shells surrounded on elastic foundations in thermal environments", *Thin-Wall. Struct.*, **117**, 178-189.

Duc, N., Quang, V.D., Nguyen, P.D. and Chien, T.M. (2018), "Nonlinear dynamic response of functional graded porous plates on elastic foundation subjected to thermal and mechanical loads", *J. Appl. Comput. Mech.*, **4**(4), 245-259.

El-Haina, F., Bakora, A., Bousahla, A.A., Tounsi, A. and Mahmoud, S.R. (2017), "A simple analytical approach for thermal buckling of thick functionally graded sandwich plates", *Struct. Eng. Mech.*, **63**(5), 585-595.

Ghorbanpour Arani, A. and Kiani, F. (2018), "Nonlinear free and forced vibration analysis of microbeams resting on the nonlinear orthotropic visco-Pasternak foundation with different boundary conditions", *Steel Compos. Struct.*, **28**(2), 149-165.

Ghorbanpour Arani, A., Haghparast, E. and Babaakbar Zarei, H. (2016), "Nonlocal vibration of axially moving graphene sheet resting on orthotropic visco-Pasternak foundation under longitudinal magnetic field", *Phys. B: Condens. Matt.*, **495**, 35-49.

Ghorbanpour Arani, A., Haghparast, E. and Zarei, H.B. (2017b), "Vibration analysis of functionally graded nanocomposite plate moving in two directions", *Steel Compos. Struct.*, **23**(5), 529-541.

Ghorbanpour Arani, A., Khoddami Maraghi, Z., Khani, M. and Alinaghian, I. (2017c), "Free vibration of embedded porous plate using third-order shear deformation and poroelasticity theories", *J. Eng.*, 1-13.

Ghorbanpour Arani, A., Maraghi, Z.K. and Ferasatmanesh, M. (2017a), "Theoretical investigation on vibration frequency of sandwich plate with PFRC core and piezomagnetic face sheets under variable in-plane load", *Struct. Eng. Mech.*, **63**(1), 65-76.

Hosseini-Hashemi, S. and Khorami, K. (2011), "Analysis of free vibrations of moderately thick cylindrical Shells made of functionally graded materials using differential quadrature method", *Modar. Mech. Eng.*, **11**(2), 93-106.

Jabbari, M., Mojahedin, A., Khorshidvand, A.R. and Eslami, M.R. (2014), "Buckling analysis of a functionally graded thin circular plate made of saturated porous materials", *J. Eng. Mech.*, **140**(2), 287-295.

Khorshidvand, A.R., Jabbari, M. and Eslami, M.R. (2012), "Thermoelastic buckling analysis of functionally graded circular plates integrated with piezoelectric layers", *J. Therm. Stress.*, **35**(8), 695-717.

Khorshidvand, A.R., Joubaneh, E.F., Jabbari, M. and Eslami, M.R. (2014), "Buckling analysis of a porous circular plate with piezoelectric sensor-actuator layers under uniform radial compression", *Acta Mech.*, **225**(1), 179-193.

Kolahdouzan, F., Gorbanpour Arani, A. and Abdollahian, M. (2018), "Buckling and free vibration analysis of FG-CNTRC-micro sandwich plate", *Steel Compos. Struct.*, **26**(3), 273-287.

Krizhevsky, G. and Stavsky, Y. (1996), "Refined theory for vibrations and buckling of laminated isotropic annular plates", *Int. J. Mech. Sci.*, **38**(5), 539–555.

Lal, R. and Ahlawat, N. (2015), "Axisymmetric vibrations and buckling analysis of functionally graded circular plates via differential transform method", *Eur. J. Mech.-A/Sol.*, **52**, 85-94.

Leclaire, P., Horoshenlov, K.V. and Cummings, A. (2001), "Transverse vibrations of a thin rectangular porous plate saturated by a fluid", *J. Sound Vibr.*, **247**(1), 1-18.

Leissa, A.W. (1969), *Vibration of Plates*, OHIO State Univ Columbus.

Liew, K.M., Han, J.B. and Xiao, Z.M. (1996), "Differential quadrature method for thick symmetric cross-ply laminates with first-order shear flexibility", *Int. J. Sol. Struct.*, **33**(18), 2647-2658.

Liew, K.M., Han, J.B., Xiao, Z.M. and Du, H. (1996), "Differential quadrature method for Mindlin plates on Winkler foundations", *Int. J. Mech. Sci.*, **38**(4), 405-421.

Loghman, A. and Cheraghbak, A. (2018), "Agglomeration effects on electro-magneto-thermo elastic behavior of nano-composite piezoelectric cylinder", *Polym. Compos.*, **39**(5), 1594-1603.

Ma, L.S. and Wang, T.J. (2003a), "Axisymmetric post-buckling of a functionally graded circular plate subjected to uniformly distributed radial compression", *Mater. Sci. For.*, **423-424**, 719-724.

Ma, L.S. and Wang, T.J. (2003b), "Nonlinear bending and post-buckling of a functionally graded circular plate under mechanical and thermal loadings", *Int. J. Sol. Struc.*, **40**(13-14), 3311-3330.

Ma, L.S. and Wang, T.J. (2004), "Relationships between axisymmetric bending and buckling solutions of FGM circular plates based on third-order plate theory and classical plate theory", *Int. J. Sol. Struct.*, **41**(1), 85-101.

Magnucka-Blandzi, E. (2008), "Axi-symmetrical deflection and buckling of circular porous-cellular plate", *Thin-Wall. Struct.*, **46**(3), 333-337.

Mohammadimehr, M., Zarei, H.B., Parakandeh, A. and Arani, A. G. (2017), "Vibration analysis of double-bonded sandwich microplates with nanocomposite facesheets reinforced by symmetric and un-symmetric distributions of nanotubes under multi physical fields", *Struct. Eng. Mech.*, **64**(3), 361-379.

Ozdemir, Y.I. (2018), "Using fourth order element for free vibration parametric analysis of thick plates resting on elastic foundation", *Struct. Eng. Mech.*, **65**(3), 213-222.

Pham, T.V. and Nguyen, D.D. (2016), "Nonlinear stability analysis of imperfect three-phase sandwich laminated polymer nanocomposite panels resting on elastic foundations in thermal environments", *VNU J. Sci.: Math. Phys.*, **32**(1), 20-36.

Quan, T.Q., Tran, P., Tuan, N.D. and Duc, N.D. (2015), "Nonlinear dynamic analysis and vibration of shear deformable eccentrically stiffened S-FGM cylindrical panels with metal-ceramic-metal layers resting on elastic foundations", *Compos. Struct.*, **126**, 16-33.

Reddy, J.N. (2004), *Mechanics of Laminated Composite Plates and Shells*, CRC Press.

Reddy, J.N., Wang, C.M. and Kitipornchai, S. (1999), "Axisymmetric bending of functionally graded circular and annular plates", *Eur. J. Mec.-A/Sol.*, **18**(2), 185-199.

Shu, C. and Richards, B.E. (1992), "Application of generalized differential quadrature to solve two-dimensional incompressible Navier-Stokes equations", *Int. J. Numer. Meth. Flu.*, **15**(7), 791-798.

Theodorakopoulos, D.D. and Beskos, D.E. (1994), "Flexural vibrations of poroelastic plates", *Acta Mech*., **103**(1-4), 191-203.

Wang, Q., Quek, S.T., Sun, C.T. and Liu, X. (2001), "Analysis of piezoelectric coupled circular plate", *Smart Mater*. *Struct*., **10**(2), 229.

Wang, X. (2008), "Changes in the natural frequency of a ferromagnetic rod in a magnetic field due to magnetoelastic interaction", *Appl*. *Math*. *Mech*., **29**(8), 1023-1032.

Wang, Y., Xu, R. and Ding, H. (2009), "Free axisymmetric vibration of FGM circular plates", *Appl*. *Math*. *Mech*., **30**(9), 1077-1082.

Wu, T., Wang, Y. and Liu, G. (2002), "Free vibration analysis of circular plates using generalized differential quadrature rule", *Comput. Meth*. *Appl*. *Mech. Eng*., **191**(46), 5365–5380.

Yahiaoui, M., Tounsi, A., Fahsi, B., Bouiadjra, R.B. and Benyoucef, S. (2018), "The role of micromechanical models in the mechanical response of elastic foundation FG sandwich thick beams", *Struct*. *Eng*. *Mech*., **68**(1), 53-66.

Zenkour, A.M. (2018), "A quasi-3D refined theory for functionally graded single-layered and sandwich plates with porosities", *Compos. Struct*., **201**, 38-48.

Zong, Z., Zhang, Y. and Zhang, Y. (2009), *Advanced Differential Quadrature Methods* (18), Chapman and Hall/CRC.

CC